1. Pinkel, D. *et al.* Differentiating juvenile myelomonocytic leukemia from infectious disease. *Blood* **91**, 365–367 (1998).
2. Loh, M.L. *et al.* Mutations in *CBL* occur frequently in juvenile myelomonocytic leukemia. *Blood* **114**, 1859–1863 (2009).
3. Muramatsu, H. *et al.* Mutations of an E3 ubiquitin ligase c-*Cbl* but not *TET2* mutations are pathogenic in juvenile myelomonocytic leukemia. *Blood* **115**, 1969–1975 (2010).
4. Pérez, B. *et al.* Genetic typing of *CBL*, *ASXL1*, *RUNX1*, *TET2* and *JAK2* in juvenile myelomonocytic leukaemia reveals a genetic profile distinct from chronic myelomonocytic leukaemia. *Br. J. Haematol.* **151**, 460–468 (2010).
5. Ng, S.B. *et al.* Exome sequencing identifies *MLL2* mutations as a cause of Kabuki syndrome. *Nat. Genet.* **42**, 790–793 (2010).
6. Minakuchi, M. *et al.* Identification and characterization of SEB, a novel protein that binds to the acute undifferentiated leukemia–associated protein SET. *Eur. J. Biochem.* **268**, 1340–1351 (2001).
7. Damm, F. *et al. SETBP1* mutations in 658 patients with myelodysplastic syndromes, chronic myelomonocytic leukemia and secondary acute myeloid leukemias. *Leukemia* **27**, 401–403 (2013).
8. Laborde, R.R. *et al. SETBP1* mutations in 415 patients with primary myelofibrosis or chronic myelomonocytic leukemia: independent prognostic impact in CMML. *Leukemia* published online; doi:10.1038/leu.2013.97 (5 April 2013).
9. Meggendorfer, M. *et al. SETBP1* mutations occur in 9% of MDS/MPN and in 4% of MPN cases and are strongly associated with atypical CML, monosomy 7, isochromosome i(17)(q10), *ASXL1* and *CBL* mutations. *Leukemia* published online; doi:10.1038/leu.2013.133 (30 April 2013).
10. Piazza, R. *et al.* Recurrent *SETBP1* mutations in atypical chronic myeloid leukemia. *Nat. Genet.* **45**, 18–24 (2013).
11. Thol, F. *et al. SETBP1* mutation analysis in 944 patients with MDS and AML. *Leukemia* published online; doi:10.1038/leu.2013.145 (7 May 2013).
12. Panagopoulos, I. *et al.* Fusion of *NUP98* and the SET binding protein 1 (*SETBP1*) gene in a paediatric acute T cell lymphoblastic leukaemia with t(11;18)(p15;q12). *Br. J. Haematol.* **136**, 294–296 (2007).
13. Cristóbal, I. *et al.* SETBP1 overexpression is a novel leukemogenic mechanism that predicts adverse outcome in elderly patients with acute myeloid leukemia. *Blood* **115**, 615–625 (2010).
14. Goyama, S. *et al.* Evi-1 is a critical regulator for hematopoietic stem cells and transformed leukemic cells. *Cell Stem Cell* **3**, 207–220 (2008).
15. Ott, M.G. *et al.* Correction of X-linked chronic granulomatous disease by gene therapy, augmented by insertional activation of *MDS1-EVI1*, *PRDM16* or *SETBP1*. *Nat. Med.* **12**, 401–409 (2006).
16. Hoischen, A. *et al. De novo* mutations of *SETBP1* cause Schinzel-Giedion syndrome. *Nat. Genet.* **42**, 483–485 (2010).
17. Yoshida, K. *et al.* Frequent pathway mutations of splicing machinery in myelodysplasia. *Nature* **478**, 64–69 (2011).
18. Flotho, C. *et al.* Genome-wide single-nucleotide polymorphism analysis in juvenile myelomonocytic leukemia identifies uniparental disomy surrounding the *NF1* locus in cases associated with neurofibromatosis but not in cases with mutant *RAS* or *PTPN11*. *Oncogene* **26**, 5816–5821 (2007).
19. Walters, D.K. *et al.* Activating alleles of *JAK3* in acute megakaryoblastic leukemia. *Cancer Cell* **10**, 65–75 (2006).
20. Sato, T. *et al.* Functional analysis of *JAK3* mutations in transient myeloproliferative disorder and acute megakaryoblastic leukaemia accompanying Down syndrome. *Br. J. Haematol.* **141**, 681–688 (2008).
21. De Vita, S. *et al.* Loss-of-function *JAK3* mutations in TMD and AMKL of Down syndrome. *Br. J. Haematol.* **137**, 337–341 (2007).
22. Norton, A. *et al.* Analysis of *JAK3*, *JAK2*, and *C-MPL* mutations in transient myeloproliferative disorder and myeloid leukemia of Down syndrome blasts in children with Down syndrome. *Blood* **110**, 1077–1079 (2007).
23. Kiyoi, H., Yamaji, S., Kojima, S. & Naoe, T. *JAK3* mutations occur in acute megakaryoblastic leukemia both in Down syndrome children and non–Down syndrome adults. *Leukemia* **21**, 574–576 (2007).
24. Elliott, N.E. *et al.* FERM domain mutations induce gain of function in JAK3 in adult T-cell leukemia/lymphoma. *Blood* **118**, 3911–3921 (2011).
25. Zhang, J. *et al.* The genetic basis of early T-cell precursor acute lymphoblastic leukaemia. *Nature* **481**, 157–163 (2012).
26. Koo, G.C. *et al.* Janus kinase 3–activating mutations identified in natural killer/T-cell Lymphoma. *Cancer Discov.* **2**, 591–597 (2012).
27. Zhang, J. *et al.* A novel retinoblastoma therapy from genomic and epigenetic analyses. *Nature* **481**, 329–334 (2012).
28. Makishima, H. *et al.* Somatic *SETBP1* mutations in myeloid malignancies. *Nat. Genet.* published online; doi:10.1038/ng.2696 (7 July 2013).
29. Crozatier, M. & Meister, M. *Drosophila* haematopoiesis. *Cell. Microbiol.* **9**, 1117–1126 (2007).
30. Changelian, P.S. *et al.* Prevention of organ allograft rejection by a specific Janus kinase 3 inhibitor. *Science* **302**, 875–878 (2003).

ONLINE METHODS

Subjects. We studied 92 children (61 boys and 31 girls) with JMML, including 7 individuals with NS/MPD, who were diagnosed as having JMML in institutions throughout Japan. Written informed consent was obtained from subjects' parents before sample collection. This study was approved by the ethics committees of the Nagoya University Graduate School of Medicine and the University of Tokyo in accordance with the Declaration of Helsinki. Diagnosis with JMML was made on the basis of internationally accepted criteria[1]. Characteristics of the 92 JMML cases are summarized in **Table 2**. The median age at diagnosis was 16 months (range of 1–160 months). Karyotypic abnormalities were detected in 16 subjects, including in 8 with monosomy 7. Fifty-six of the 92 subjects (61%) received allogeneic HSCT.

Sample preparation. Genomic DNA was extracted using the QIAamp DNA Blood Mini kit and the QIAamp DNA Investigator kit (Qiagen) according to the manufacturer's instructions. The T Cell Activation/Expansion kit, human (Miltenyi Biotec) was used for the expansion of $CD3^+$ T cells from subjects' peripheral blood or bone marrow mononuclear cells[3].

Whole-exome sequencing. Exome capture from paired tumor-reference DNA was performed using SureSelect Human All Exon V3 (Agilent Technologies), covering 50 Mb of coding exons, according to the manufacturer's protocol. Enriched exome fragments were subjected to massively parallel sequencing using the HiSeq 2000 platform (Illumina). Candidate somatic mutations were detected through our in-house pipeline (Genomon) as previously described[17].

Detection of mutations from whole-exome sequencing data. Detection of candidate somatic mutations was performed according to previously described algorithms with minor modifications[17]. Briefly, the number of reads containing single-nucleotide variations (SNVs) and indels in both tumor and reference samples was determined using SAMtools[31], and the null hypothesis of equal allele frequencies in tumor and reference samples was tested using the two-tailed Fisher's exact test. A variant was adopted as a candidate somatic mutation if it had $P < 0.01$, if it was observed in bidirectional reads (in both plus and minus strands of the reference sequence) and if its allele frequency was less than 0.25 in the corresponding reference sample. For the detection of germline mutations in RAS pathway genes, SNVs and indels having allele frequencies of more than 0.25 (SNVs) and 0.10 (indels) were interrogated for 46 genes, which consisted of known JMML-related RAS pathway genes and genes registered in the pathway databases ('Ras signaling pathway' in BioCarta and 'signaling to RAS' in Reactome[32]). For variant calls in tumor samples for which the paired normal reference was not available, candidate variants in the RAS pathway were detected at an allele frequency of >0.10. Finally, the list of candidate somatic and/or germline mutations was generated by excluding synonymous SNVs and other variants registered in either dbSNP131 or an in-house SNP database constructed from 180 individual samples. All candidates were validated by Sanger sequencing as previously described.

Estimation of tumor content. The tumor content of bone marrow specimens was estimated from the allele frequency of the somatic mutations identified by deep sequencing. For homozygous mutations, as indicated by an allele frequency of >0.75, the tumor content (F_{tumor}) was calculated from the observed frequency ($F_{observed}$) of the mutation according to the following equation: $F_{tumor} = 2 \times F_{observed} - 1$. For heterozygous mutations, the tumor content was calculated by doubling the allele frequency.

Power analysis of whole-exome sequencing. The power of detecting somatic mutations at each nucleotide position in whole-exome sequencing was estimated by Monte-Carlo simulation ($n = 1{,}000$) on the basis of the observed mean depth of coverage for each exon in germline and tumor samples and the observed tumor content for each sample, which were estimated using the allele frequencies of the observed mutations. For the samples with no observed somatic mutations, the average tumor content of the informative samples was employed. Simulations were performed across a total of 192,424 exons.

Copy number analysis in whole-exome sequencing data. To detect copy number lesions at a single-exon level, the mean coverage of each exon normalized by the mean depth of coverage of the entire sample was compared with that of 12 unrelated normal DNA samples. Exons showing normalized coverage greater than 3 s.d. from the mean coverage of the reference samples were called as candidates for copy number alterations. All candidate exons of RAS pathway genes were visually inspected using the Integrative Genomics Viewer[33] and were validated by Sanger sequencing of corresponding putative breakpoint-containing fragments.

Targeted deep sequencing. Deep sequencing of the targeted genes was performed essentially as described in the 'deep sequencing of pooled target exons' section in ref. 17, except that target DNA was not pooled. Briefly, all exons of *PTPN11*, *NF1*, *KRAS*, *NRAS*, *CBL*, *SETBP1*, *JAK3* and *SH3BP1* were PCR amplified with Quick Taq HS DyeMix (TOYOBO) and the PrimeSTAR GXL DNA Polymerase kit (Takara Bio) using primers including the NotI restriction site (**Supplementary Table 3**). The PCR products from an individual sample were combined and purified with the QIAquick PCR Purification kit (Qiagen) for subsequent digestion with NotI (Fermentas). Digested PCR product was purified, concatenated with T4 DNA ligase (Takara Bio) and sonicated to generate fragments with an average size of 150 bp using Covaris. Fragments were processed for sequencing according to a modified Illumina paired-end library protocol, and sequences were read by a HiSeq 2000 instrument using a 100-bp paired-end read protocol.

Variant calls in targeted deep sequencing. Data processing and variant calling were performed with modifications to the protocol described in a previous publication[17]. Each read was aligned to the set of targeted sequences from PCR amplification, with BLAT[34] instead of Burrows-Wheeler Aligner (BWA)[35] used with the -fine option. Mapping information in the .psl format was converted to the .sam format with paired-read information. Of the successfully mapped reads, reads were excluded from further analysis if they mapped to multiple sites, mapped with more than four mismatched bases or had more than ten soft-clipped bases. Next, the Estimation_CRME script was run to eliminate strand-specific errors and exclude PCR-derived errors. A strand-specific mismatch ratio was calculated for each nucleotide variant for both strands using the bases from read cycles 11 to 50 on the next-generation sequencer. By excluding the top five cycles showing the highest mismatch rates, strand-specific mismatch rates were recalculated, and the smaller value between both strands was adopted as a nominal mismatch ratio for that variant. After excluding variants found in dbSNP131 or the in-house SNP database, non-silent variants having a mismatch ratio of greater than 0.05 were called as candidates, unless they had median values of the mismatch ratio at the relevant nucleotide positions in the 92 samples of greater than 0.01, as such variants were likely to be caused by systematic PCR problems. Finally, candidates with mismatch ratios of >0.15 were further validated by Sanger sequencing.

Annotation of the detected mutations. Detected mutations were annotated using ANNOVAR[36]. The positions of the mutations were based on the following RefSeq transcript sequences: NM_002834.3 for *PTPN11*, NM_000267.3 for *NF1*, NM_002524.4 for *NRAS*, NM_004985.3 for *KRAS*, NM_005188.3 for *CBL*, NM_015559.2 for *SETBP1* and NM_000215.3 for *JAK3*. The effect of the mutations on protein function was assessed by SIFT[37], PolyPhen-2 (ref. 38) and MutationTaster[39].

Whole-genome sequencing. Paired tumor-reference DNA samples were sequenced with the HiSeq 2000 platform according to the manufacturer's instructions to obtain 30× read coverage for reference samples and 40× coverage for tumor samples. Obtained FASTQ sequences were aligned to the human reference genome (hg19) using BWA[35] 0.5.8 with default parameters. Alignment of pairs of sequences, at least one of which was not mapped or was considered to have possible mapping problems (with mapping quality of less than 40, insertions or deletions, soft-clipped sequence of more than 10% of the length of the original sequence, irregular paired-read orientation or mate distance of greater than 2,000 bp), was attempted with BLAT[34] using default parameters, except for stepSize = 5 and repMatch = 2,253. Mapping statistics were calculated by counting the bases at each genomic position with SAMtools[31]. For variant calling, variant and reference bases with base quality of >30 were counted in both germline and tumor samples, and the Fisher's

exact test was applied. Variants with P of <0.01 were called. Variants having allele frequency of >0.25 in the germline sample were excluded. Variants found in 12 unrelated germline samples with an allele frequency of >0.01 on average were also excluded owing to the high probability that they represented false positive calls. Copy number estimation was performed by calculating the averaged ratio of read depths in germline and tumor samples in 10,000-base bins. An allele-specific copy number plot was generated by measuring the allele frequency of the tumor sample at the positions in which more than 25% of the allele mismatch was observed in germline samples. For the detection of chromosomal structural variations, soft-clipped sequences that could be mapped to a unique genomic position were selected. Structural variation candidates that had more than four supporting read pairs in total and at least one read pair from each side of the breakpoint were called. Contig sequences were generated by assembling the reads within 200 bp of the breakpoint with CAP3 (ref. 40), and structural variations having the contig sequence that could be aligned to the alternate assembly of the hg19 genome with more than 93% identity were excluded as false positives. Structural variations with read depth of greater than 150 on at least one side of the breakpoint were considered to be mapped to a repeat element and were also excluded. For detection of viruses, unmapped sequences were aligned to the collection of all viral genomes in the RefSeq database using BLAT. A virus was considered to be detected if its genome was covered by mean read coverage of >1.

cDNA sequencing. Total RNA was extracted using the RNeasy Mini kit (Qiagen) and was reverse transcribed with the ThermoScript RT-PCR system (Life Technologies). Target sequences were PCR amplified with the PrimeSTAR GXL DNA Polymerase kit using the primers listed in **Supplementary Table 3** and were sequenced.

Statistical analysis. For comparison of the frequency of mutations or other clinical features between disease groups, categorical variables were analyzed using the Fisher's exact test, and continuous variables were tested using the Mann-Whitney U test. Overall survival and transplantation-free survival were estimated by the Kaplan-Meier method. Hazard ratios for survival with 95% CIs were estimated according to the Cox proportional hazards model, and difference in survival was tested by log-rank test. STATA version 12.0 (StataCorp) was used for all statistical calculations.

31. Li, H. *et al.* The Sequence Alignment/Map format and SAMtools. *Bioinformatics* **25**, 2078–2079 (2009).
32. Matthews, L. *et al.* Reactome knowledgebase of human biological pathways and processes. *Nucleic Acids Res.* **37**, D619–D622 (2009).
33. Thorvaldsdóttir, H., Robinson, J.T. & Mesirov, J.P. Integrative Genomics Viewer (IGV): high-performance genomics data visualization and exploration. *Brief. Bioinform.* **14**, 178–192 (2013).
34. Kent, W.J. BLAT—the BLAST-like alignment tool. *Genome Res.* **12**, 656–664 (2002).
35. Li, H. & Durbin, R. Fast and accurate short read alignment with Burrows-Wheeler transform. *Bioinformatics* **25**, 1754–1760 (2009).
36. Wang, K., Li, M. & Hakonarson, H. ANNOVAR: functional annotation of genetic variants from high-throughput sequencing data. *Nucleic Acids Res.* **38**, e164 (2010).
37. Kumar, P., Henikoff, S. & Ng, P.C. Predicting the effects of coding non-synonymous variants on protein function using the SIFT algorithm. *Nat. Protoc.* **4**, 1073–1081 (2009).
38. Adzhubei, I.A. *et al.* A method and server for predicting damaging missense mutations. *Nat. Methods* **7**, 248–249 (2010).
39. Schwarz, J.M., Rödelsperger, C., Schuelke, M. & Seelow, D. MutationTaster evaluates disease-causing potential of sequence alterations. *Nat. Methods* **7**, 575–576 (2010).
40. Huang, X. & Madan, A. CAP3: A DNA sequence assembly program. *Genome Res.* **9**, 868–877 (1999).

blood

2013 121: 862-863
doi:10.1182/blood-2012-11-465633

Rabbit antithymocyte globulin and cyclosporine as first-line therapy for children with acquired aplastic anemia

Yoshiyuki Takahashi, Hideki Muramatsu, Naoki Sakata, Nobuyuki Hyakuna, Kazuko Hamamoto, Ryoji Kobayashi, Etsuro Ito, Hiroshi Yagasaki, Akira Ohara, Akira Kikuchi, Akira Morimoto, Hiromasa Yabe, Kazuko Kudo, Ken-ichiro Watanabe, Shouichi Ohga and Seiji Kojima

Blood (print ISSN 0006-4971, online ISSN 1528-0020), is published weekly by the American Society of Hematology, 2021 L St, NW, Suite 900, Washington DC 20036.

To the editor:

Rabbit antithymocyte globulin and cyclosporine as first-line therapy for children with acquired aplastic anemia

Horse antithymocyte globulin (hATG) and cyclosporine have been used as standard therapy for children with acquired aplastic anemia (AA) for whom an HLA-matched family donor is unavailable. However, in 2009, hATG (lymphoglobulin; Genzyme) was withdrawn and replaced by rabbit ATG (rATG; thymoglobulin; Genzyme) in Japan. Many other countries in Europe and Asia are facing the same situation.[1] Marsh et al recently reported outcomes for 35 adult patients with AA who were treated with rATG and cyclosporine as a first-line therapy.[2] Although the hematologic response rate was 40% at 6 months, several patients subsequently achieved late responses. The best response rate was 60% compared with 67% in a matched-pair control group of 105 patients treated with hATG. The overall and transplantation-free survival rates appeared to be significantly inferior with rATG compared with hATG at 68% versus 86% ($P = .009$) and 52% versus 76% ($P = .002$), respectively. These results are comparable to those from a prospective randomized study reported by Scheinberg et al comparing hATG and rATG.[3] Both studies showed the superiority of hATG over rATG.[2,3]

We recently analyzed outcomes for 40 Japanese children (median age, 9 years; range, 1-15) with AA treated using rATG and cyclosporine. The median interval from diagnosis to treatment was 22 days (range, 1-203). The numbers of patients with very severe, severe, and nonsevere disease were 14, 10, and 16, respectively. The ATG dose was 3.5 mg/kg/day for 5 days. The median follow-up time for all patients was 22 months (range, 6-38). At 3 months, no patients had achieved a complete response (CR) and partial response (PR) was seen in only 8 patients (20.0%). At 6 months, the numbers of patients with CR and PR were 2 (5.0%) and 17 (42.5%), respectively. After 6 months, 5 patients with PR at 6 months had achieved CR and 4 patients with no response at 6 months had achieved PR, offering a total best response rate of 57.5%. Two patients relapsed at 16 and 19 months without receiving any second-line treatments. Two patients with no response received a second course of rATG at 13 and 17 months, but neither responded. Sixteen patients underwent hematopoietic stem cell transplantation (HSCT) from alternative donors (HLA-matched unrelated donors, n = 13; HLA-mismatched family donors, n = 3). Two deaths occurred after rATG therapy, but no patients died after HSCT. Causes of death were intracranial hemorrhage at 6 months and acute respiratory distress syndrome at 17 months. The overall 2-year survival rate was 93.8% and the 2-year transplantation-free survival rate was 50.3% (Figure 1).

In our previous prospective studies with hATG, the response rates after 6 months were 68% and 70%, respectively, with no increases in response rates observed after 6 months.[4,5] Our results support the notion that rATG is inferior to hATG for the treatment of AA in children. First-line HSCT from an alternative donor may be justified, considering the excellent outcomes in children who received salvage therapies using alternative donor HSCT.

Yoshiyuki Takahashi
Department of Pediatrics, Nagoya Graduate School of Medicine, Nagoya, Japan

Hideki Muramatsu
Department of Pediatrics, Nagoya Graduate School of Medicine, Nagoya, Japan

Naoki Sakata
Department of Pediatrics, Kinki University School of Medicine, Osaka, Japan

Nobuyuki Hyakuna
Center of Bone Marrow Transplantation, Ryukyu University Hospital, Okinawa, Japan

Kazuko Hamamoto
Department of Pediatrics, Hiroshima Red Cross Hospital, Hiroshima, Japan

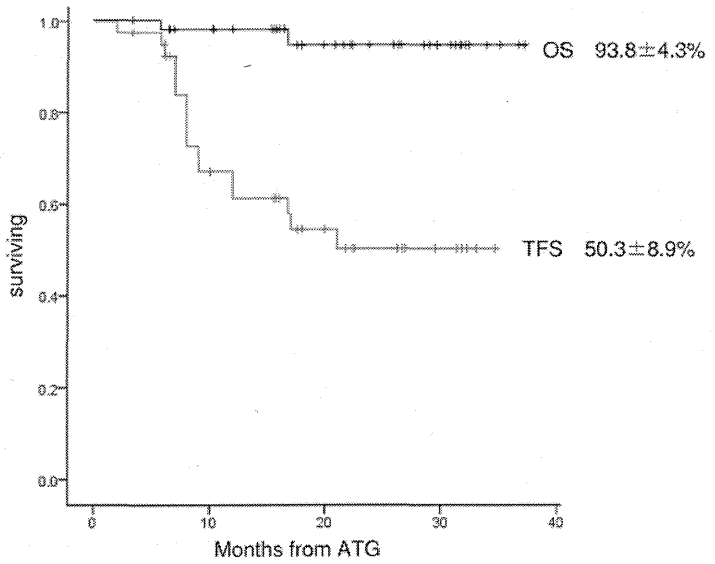

Figure 1. Kaplan-Meier estimates of overall survival (OS) and transplantation-free survival (TFS) in 40 Japanese children with AA. Survival was investigated using Kaplan-Meier methods. OS for all patients with AA after rATG and cyclosporine as first-line therapy included patients who later received HSCT for nonresponse to rATG. In the analysis of TFS for all patients treated with rATG and CSA, transplantation was considered an event.

Ryoji Kobayashi
Department of Pediatrics, Sapporo Hokuyu Hospital, Sapporo, Japan

Etsuro Ito
Department of Pediatrics, Hirosaki University School of Medicine, Hirosaki, Japan

Hiroshi Yagasaki
Department of Pediatrics, School of Medicine, Nihon University, Tokyo, Japan

Akira Ohara
Division of Blood Transfusion, Toho University Omori Hospital, Tokyo, Japan

Akira Kikuchi
Department of Pediatrics, Teikyo University School of Medicine, Tokyo, Japan

Akira Morimoto
Department of Pediatrics, Jichi Medical University School of Medicine, Tochigi, Japan

Hiromasa Yabe
Department of Cell Transplantation and Regenerative Medicine, Tokai University School of Medicine, Isehara, Japan

Kazuko Kudo
Division of Hematology and Oncology, Shizuoka Children's Hospital, Shizuoka, Japan

Ken-ichiro Watanabe
Department of Pediatrics, Graduate School of Medicine, Kyoto University, Kyoto, Japan

Shouichi Ohga
Department of Perinatal and Pediatric Medicine, Graduate School of Medical Sciences, Kyushu University, Fukuoka, Japan

Seiji Kojima
Department of Pediatrics, Nagoya Graduate School of Medicine, Nagoya, Japan

on behalf of the Japan Childhood Aplastic Anemia Study Group

Conflict-of-interest disclosure: The authors declare no competing financial interests.

Correspondence: Dr Seiji Kojima, Nagoya Graduate School of Medicine, Tsurumai-cho 65, Showa-ku, Nagoya, Ai, Japan 466-8550; e-mail: kojimas@med.nagoya-u.ac.jp.

References

1. Dufour C, Bacigalupo A, Oneto R, et al. Rabbit ATG for aplastic anaemia treatment: a backward step? *Lancet.* 2011;378(9806):1831-1833.
2. Marsh JC, Bacigalupo A, Schrezenmeier H, et al. Prospective study of rabbit antithymocyte globulin and cyclosporine for aplastic anemia from the EBMT Severe Aplastic Anaemia Working Party. *Blood.* 2012;119(23):5391-5396.
3. Scheinberg P, Nunez O, Weinstein B, et al. Horse versus rabbit antithymocyte globulin in acquired aplastic anemia. *N Engl J Med.* 2011;365(5):430-438.
4. Kojima S, Hibi S, Kosaka Y, et al. Immunosuppressive therapy using antithymocyte globulin, cyclosporine, and danazol with or without human granulocyte colony-stimulating factor in children with acquired aplastic anemia. *Blood.* 2000;96(6):2049-2054.
5. Kosaka Y, Yagasaki H, Sano K, et al. Prospective multicenter trial comparing repeated immunosuppressive therapy with stem-cell transplantation from an alternative donor as second-line treatment for children with severe and very severe aplastic anemia. *Blood.* 2008;111(3):1054-1059.

To the editor:

Peripheral blood stem cells versus bone marrow in pediatric unrelated donor stem cell transplantation

The relative benefits and risks of peripheral blood stem cells (PBSCs) versus bone marrow (BM) for allogeneic hematopoietic stem cell transplantation (SCT) are still a matter of highly controversial debates.[1-3] The first randomized study comparing the 2 stem cell sources in unrelated donor SCT recently documented comparable overall and event-free survival, but indicated a higher risk for chronic graft-versus-host disease (GVHD) with PBSCs.[4] Only a few pediatric patients were included in this study even though the long-term sequelae of chronic GVHD are of particular concern in this patient group.

We retrospectively compared the long-term outcome of contemporaneous unrelated donor SCT in 220 children transplanted with BM (n = 102) or PBSCs (n = 118) for hematologic malignancies and reported to the German/Austrian pediatric registry for SCT. All patients had received myeloablative conditioning followed by unmanipulated SCT from HLA-matched unrelated donors. The PBSC and BM groups were comparable with regard to patient and donor age, sex, cytomegalovirus (CMV) serostatus, disease status at transplantation, GVHD prophylaxis, growth factor use, and degree of HLA matching. The groups differed with regard to disease category with slightly more myelodysplastic syndrome patients ($P = .02$) and a higher CD34-cell dose ($P = .001$) in the PBSC group.

Neutrophil and platelet engraftment were achieved significantly faster after PBSC than BM transplantation (Figure 1A-B). In this entirely pediatric cohort, the incidence of clinically relevant grade II-IV acute GVHD (Figure 1C) did not differ. Most importantly, the incidence of chronic GVHD (PBSCs vs BM: 35% vs 33%, respectively; $P = .9$) and extensive chronic GVHD (Figure 1D) proved low and was virtually identical in the 2 groups. With a median follow-up time of 3 years, overall survival (PBSCs vs BM: 50% ± 5% vs 46% ± 6%, respectively; $P = .63$) and event-free survival (PBSCs vs BM: 45% ± 5% vs 44% ± 6%, respectively; $P = .59$) were comparable (Figure 1E-F). In multivariable analysis, taking into account all parameters with $P < .2$ in univariate analysis, the only significant independent risk factor for treatment failure was advanced disease status at the time of transplantation (relative risk = 2.4, 95% confidence interval, 1.5-3.8; $P = .001$). In contrast, stem cell source (PBSCs vs BM) had no effect (relative risk = 1.1, 95% confidence interval, 0.7-1.6; $P = .8$).

Our registry-based analysis provides evidence that in pediatric recipients of HLA-matched unrelated-donor transplantation with consistent antithymocyte globulin (ATG) use during conditioning, transplantation with PBSCs and BM results in comparable clinical outcomes without detectable differences in the risk of acute or, more importantly, chronic GVHD. Consistent with a recent study underscoring the role of ATG for the prevention of acute and chronic GVHD,[5] the use of ATG in 96% of our transplantation procedures compared with only 27% in the above-mentioned randomized study by Anasetti et al[4] might be one of the key factors responsible for the overall low and comparable incidence of

Heterozygosity for the Y701C *STAT1* mutation in a multiplex kindred with multifocal osteomyelitis

Osamu Hirata,[1] Satoshi Okada,[1,2] Miyuki Tsumura,[1] Reiko Kagawa,[1] Mizuka Miki,[1] Hiroshi Kawaguchi,[1] Kazuhiro Nakamura,[1] Stéphanie Boisson-Dupuis,[2,3] Jean-Laurent Casanova,[2,3] Yoshihiro Takihara,[4] and Masao Kobayashi[1]

[1]Department of Pediatrics, Hiroshima University Graduate School of Biomedical & Health Sciences, Hiroshima, Japan; [2]St. Giles Laboratory of Human Genetics of Infectious Diseases, Rockefeller Branch, The Rockefeller University, New York, NY, USA; [3]Laboratory of Human Genetics of Infectious Diseases, Necker Branch, Inserm U980 and University Paris Descartes, Necker Medical School, Paris, France, EU; [4]Department of Stem Cell Biology, Research Institute for Radiation Biology and Medicine, Hiroshima University, Hiroshima, Japan

ABSTRACT

Heterozygosity for dominant-negative *STAT1* mutations underlies autosomal dominant Mendelian susceptibility to mycobacterial diseases. Mutations conferring Mendelian susceptibility to mycobacterial diseases have been identified in the regions of the *STAT1* gene encoding the tail segment, DNA-binding domain and SH2 domain. We describe here a new heterozygous mutation, Y701C, in a Japanese two-generation multiplex kindred with autosomal dominant Mendelian susceptibility to mycobacterial diseases. This mutation affects precisely the canonical STAT1 tyrosine phosphorylation site. The Y701C STAT1 protein is produced normally, but its phosphorylation is abolished, resulting in a loss-of-function for STAT1-dependent cellular responses to interferon-γ or interferon-α. In the patients' cells, the allele is dominant-negative for γ-activated factor-mediated responses to interferon-γ, but not for interferon-stimulated gene factor-3-mediated responses to interferon-α/β, accounting for the clinical phenotype of Mendelian susceptibility to mycobacterial diseases without severe viral diseases. Interestingly, both patients displayed multifocal osteomyelitis, which is often seen in patients with Mendelian susceptibility to mycobacterial diseases with autosomal dominant partial IFN-γR1 deficiency. Multifocal osteomyelitis should thus prompt investigations of both STAT1 and IFN-γR1. This experiment of nature also confirms the essential role of tyrosine 701 in human STAT1 activity *in natura*.

Introduction

Mendelian susceptibility to mycobacterial diseases (MSMD) (OMIM 209950) is a rare congenital disorder characterized by susceptibility to clinical diseases caused by weakly virulent mycobacteria, such as *Mycobacterium bovis* Bacille Calmette-Guérin (BCG) and non-tuberculous mycobacteria.[1,2] Affected individuals are also susceptible to *M. tuberculosis*, a more virulent mycobacterial species.[3] Nine MSMD-causing genes (*IFNGR1*, *IFNGR2*, *IL12B*, *IL12RB1*, *ISG15*, *STAT1*, *IRF8*, *CYBB* and *NEMO*) defining 17 different genetic etiologies have been identified to date.[4-11] Mutations of *IL12B*, *IL12RB1* and *NEMO* impair the production of interferon (IFN)-γ, whereas mutations of *IFNGR1*, *IFNGR2* and *STAT1* impair cellular responses to IFN-γ. Moreover, autosomal recessive (AR) ISG15 deficiency has recently been identified as a genetic cause of MSMD.[11] A lack of ISG15 secretion by leukocytes results in impaired IFN-γ production by NK and T lymphocytes, accounting for mycobacterial disease. Thus, single-gene variants disrupting IL-12- or ISG15-dependent, IFN-γ-mediated immunity result in an inherited predisposition to mycobacterial infections.[12,13] However, no genetic etiology has yet been established for about half the patients with MSMD.

The first identification of MSMD-causing mutations of *STAT1* in 2001 was surprising, because STAT1 is involved in cellular responses mediated by cytokines other than IFN-γ, including IFN-α/β in particular. IFN-γ stimulation results in the phosphorylation of STAT1 on tyrosine 701, inducing its homodimerization to form gamma-activated factor (GAF). GAF binds the gamma-activated sequence (GAS) to induce the transcription of target genes involved in antimycobacterial immunity. On the other hand, IFN-α/β stimulation induces the phosphorylation of both STAT1 and STAT2, resulting in the formation of the heterotrimeric IFN-stimulated gene factor-3 (ISGF3) complex with IRF9. ISGF3 recognizes IFN-stimulated response element (ISRE) motifs in target genes and their expression confers anti-viral immunity. Indeed, heterozygosity for STAT1 dominant-negative alleles is responsible for AD MSMD.[14-17] Six mutations, *E320Q*, *Q463H*, *K637E*, *M654K*, *K673R* and *L706S* in *STAT1*, have been reported (Figure 1A).[14-17] The L706S mutation affects the tail segment domain of STAT1, abolishing phosphorylation at Y701.[14] The E320Q and Q463H mutations affect the DNA-binding domain.[15] They have no effect on STAT1 phosphorylation, but modify the DNA-binding capacity of GAF, impairing

 doi:10.3324/haematol.2013.083741
OH and SO contributed equally to this manuscript.
The online version of this article has a Supplementary Appendix.
Manuscript received on January 6, 2013. Manuscript accepted on April 5, 2013.
Correspondence: masak@hiroshima-u.ac.jp

STAT1-dependent immunity. The other three mutations affect the SH2 domain. The M654K and K673R mutations impair the tyrosine phosphorylation of STAT1, whereas the K637E mutation impairs both STAT1 phosphorylation and GAF-DNA binding.[16,17] These mutations are loss-of-function or hypomorphic and have been shown to exert a dominant-negative effect on wild-type STAT1 for IFN-γ responses.[14,15] We report here the molecular and clinical features of a multiplex kindred with MSMD due to a new *STAT1* allele, with a mutation of the tyrosine 701 codon.

Methods

Case report

The patient (P1) is a 5-year old Japanese boy born to a non-consanguineous family (Figure 1B). At the age of 2 months he presented with a mild fever and rash. Initial laboratory tests demonstrated leukocytosis (28.9x10^9/L) with eosinophilia (11.1x10^9/L) and a mild acute-phase inflammatory response. Treatment with cefotaxime was initiated and the patient's symptoms improved over the first 2 days, but leukocytosis with eosinophilia persisted for 2 weeks. No bacteria could be cultured from blood, the pharynx or stool samples. P1 was vaccinated with BCG at the age of 4 months. At the age of 3 years, he suffered severe back pain and dysbasia. Laboratory tests revealed mild leukocytosis (13.9x10^9/L) and high levels of C-reactive protein (3.99 mg/dL) and immunoglobulin (IgG; 2070 mg/dL) in the serum. Magnetic resonance imaging and whole-body bone scintigraphy revealed multifocal osteomyelitis in three vertebrae and the cranial, costal, clavicular, bilateral tibial and pelvic bones. Histological findings for the tibial bone were suggestive of tuberculoid granulomas, but no pathogenic bacteria, including *Mycobacterium*, were detected in the tissues by polymerase chain reaction or culture. The patient's leukocytes displayed a normal oxidative burst and normal proliferation in response to stimulation with phytohemagglutinin and concanavalin A. *STAT1* sequencing revealed a heterozygous nucleotide substitution (2102 A>G) in exon 23, resulting in the substitution of a cysteine for a tyrosine residue at amino-acid position 701 (Y701C). The patient (P1) started treatment with antimycobacterial drugs, including rifampicin, sulfamethoxazole/trimethoprim and clarithromycin. The clinical symptoms and laboratory parameters responded well to the treatment. These treatments have been maintained ever since, with the patient now being 5 years old. The patient has had no episodes of severe viral infection. He has had mumps, chicken pox and flu, but all these diseases followed a normal clinical course. Normal levels of specific antibodies against these viruses were detected in P1 (*Online Supplementary Table S1*). He has not yet been vaccinated against measles and rubella.

His mother (P2) was vaccinated with BCG in infancy without complications. She had a history of multifocal osteomyelitis in the frontal bone, right maxilla, multiple vertebral bodies and ribs at 18 years of age. Initial laboratory tests showed a moderate acute-phase inflammatory response. Histological findings in the costal bone were consistent with a granulomatous change. No pathogenic bacteria were detected. P2 was treated with levofloxacin hydrate and loxoprofen for 2 years. These treatments improved, but did not cure the symptoms. After this episode, P2 suffered from recurrent cervical and back pain. At the age of 38, confluent changes in the pressure on cervical and lumbar vertebrae were detected on plain X ray, as a sequel of multifocal osteomyelitis. Since the identification of a heterozygous Y701C *STAT1* mutation in the family study, P2 has been treated with rifampicin, sulfamethoxazole/trimethoprim and clarithromycin. This treatment appears to be effective, as the recurrent bone pain disappeared after treatment initiation. P2 presented no signs suggestive of immunodeficiency during childhood. She had no history of severe viral infections and normal levels of the specific antibodies against Epstein-Barr, chicken pox, mumps, rubella and measles viruses (*Online Supplementary Table S1*).

We obtained blood samples from the patients, relatives, and healthy adult controls, after obtaining informed consent. This study was approved by the Ethics Committee/Internal Review Board of Hiroshima University.

The experimental methods are described in detail in the *Online Supplementary Methods* section.

Results

Identification of a new STAT1 mutation

High-molecular weight genomic DNA was extracted from peripheral blood. The exons and the flanking introns of genes responsible for MSMD, including *STAT1*, *IFNGR1*, *IFNGR2*, *IL12B*, *IL12RB1* and *NEMO*, were amplified by PCR and analyzed by Sanger sequencing. We identified a new heterozygous mutation, 2102 A>G (Y701C), in exon 23 of *STAT1* in P1 (Figure 1B). The Y701C mutation was not found in the National Center for Biotechnology Information, Ensembl or dbSNP databases, or in our own in-house database of 621 exomes. We also sequenced *STAT1* in 1,052 controls from 52 ethnic groups from the *Centre d'Etude du Polymorphisme Humain* and Human Genome Diversity panels; Y701C was not detected in these controls. This mutation was therefore considered to be a rare variant rather than an irrelevant polymorphism. Familial segregation analysis identified the same mutation in the subject's mother (P2), whereas the father and older brother were both wild-type and healthy. The mother had a history of multiple osteomyelitis of unknown etiology at 18 years of age, revealing an AD pattern of segregation of the MSMD clinical phenotype with heterozygosity for the *STAT1* allele. Figure 1A shows previously identified heterozygous or biallelic *STAT1* mutations causing AD or AR genetic susceptibility to mycobacterial diseases.[14-22] The Y701C mutation affects the Y701 residue, the site of tyrosine phosphorylation in the STAT1 tail segment domain, a residue crucial for the activation of this molecule.[23,24]

STAT1 phosphorylation and cytokine production by peripheral blood mononuclear cells in response to interferon-γ stimulation

Interferon-γR1 is expressed ubiquitously, at moderate levels, on the cell surface, whereas very little IFN-γR2 is present and the expression of this receptor is tightly regulated, both spatially and temporally. Thus, IFN-γR2 is thought to be the factor determining responsiveness to IFN-γ.[25-27] The CD14-positive monocytes in peripheral blood are known to express relatively high levels of IFN-γR2.[28] We, therefore, investigated the cellular response to IFN-γ, focusing on CD14-positive monocytes. We purified CD14-positive monocytes by magnetic sorting and incubated them in the presence of lipopolysaccharide and various concentrations of IFN-γ. We then collected the supernatant, in which we determined tumor necrosis factor (TNF) levels. TNF production was severely impaired in the patients (P1 and P2), regardless of the dose of IFN-γ used for stimulation (Figure 1C). We analyzed STAT1 phospho-

rylation in response to IFN-γ by flow cytometry. STAT1 phosphorylation levels were lower in CD14-positive monocytes from patients than in control cells (Figure 1D). The CD14-positive monocytes of both patients displayed severe impairment of TNF production in the presence of lipopolysaccharide and IFN-γ, probably due to the impairment of Y701 phosphorylation in response to IFN-γ stimulation.

STAT1 phosphorylation and DNA-binding ability in Epstein-Barr virus-B cells

We assessed STAT1 production and phosphorylation in

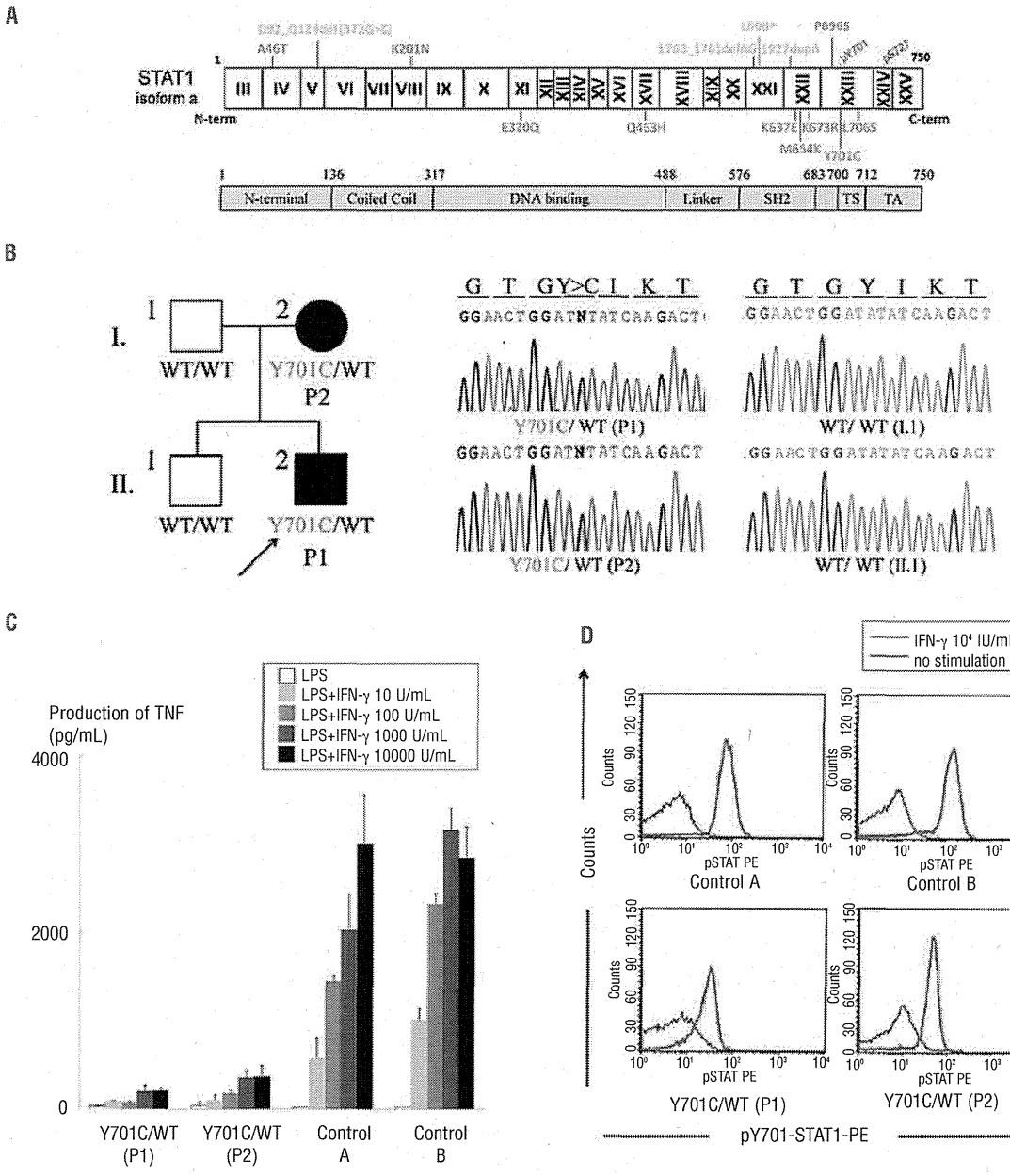

Figure 1. (A) Summary of loss-of-function *STAT1* mutations. The N-terminal domain, coiled-coil domain, DNA-binding domain, linker domain, SH2 domain, tail segment domain (TS), and transactivation domain (TA) are shown, together with Y701, the site of tyrosine phosphorylation. The dominant-negative mutants (blue) are indicated below the protein and the recessive forms of hypomorphic (green) and loss-of-function mutations (yellow) are shown above the protein. Y701C is shown in red. (B) The heterozygous Y701C mutation was detected in the patient (II.2) and his mother (I.2). Closed symbols indicate an affected individual and open symbols indicate a healthy family member. (C) CD14-positive monocytes were incubated in the presence of lipopolysaccharide (LPS) (100 ng/mL) and various concentrations of IFN-γ for 48 h and TNF production was then analyzed. CD14-positive monocytes from the patients (P1 and P2) produced abnormally small amounts of TNF. Two independent experiments were performed. (D) Flow cytometry analysis of STAT1 phosphorylation upon IFN-γ stimulation, on peripheral monocytes ($CD14^+$ gate). STAT1 phosphorylation levels were lower in the patients' cells than in control cells. The black line indicates an absence of stimulation and the red line, stimulation with 10^4 IU/mL IFN-γ. Three independent experiments were performed.

Epstein-Barr virus (EBV)-B cells from a healthy control (WT/WT), P1 (Y701C/WT), another patient with AD STAT1 deficiency (L706S/WT) and a patient with complete STAT1 deficiency (1760_1761delAG/1760_1761delAG, -/-), by immunoblotting (Figure 2A).[14,20,21] STAT1 protein levels were normal in all EBV-B cells except those from a patient with complete STAT1 deficiency. However, STAT1 phosphorylation in response to stimulation with interferons was weak, but not abolished, in EBV-B cells carrying Y701C or L706S mutations. The DNA-binding ability of the mutant STAT1 proteins was analyzed by electrophoretic mobility shift assay on EBV-B cells. EBV-B cells containing the Y701C or L706S STAT1 proteins displayed a partial impairment of GAF DNA-binding in response to stimulation with interferons (Figure 2C). The GAF-DNA binding complexes were shown, by supershift analysis, to consist of STAT1 homodimers, STAT3 homodimers and STAT1/3 heterodimers, following stimulation with IFN-γ and IFN-α, respectively (*data not shown*). As previously described, GAF was unable to bind DNA in response to IFN-γ in EBV-B cells from a patient with complete STAT1 deficiency.[20] However, a complex identified as STAT3 homodimers was visible following incubation with IFN-α. By contrast, ISRE binding to DNA following IFN-α stimulation was found to be similar in cells from the patients and cells from controls, except for complete STAT1 deficiency. STAT1 phosphorylation and GAF DNA binding in EBV-B cells were impaired to a similar extent in P1 and P2 (*Online Supplementary Figure S1B,C*). Overall, EBV-B cells from the patients displayed impaired, but not abolished, STAT1 phosphorylation in response to stimulation with interferons, resulting in the partial impairment of GAF-DNA binding. However, ISRE-DNA binding levels in response to IFN-α stimulation were unaffected.

The phosphorylation and nuclear translocation of Y701C STAT1 are impaired

We transiently introduced WT and mutant *STAT1* into U3C cells by lipofection, and analyzed, by immunoblotting, the tyrosine 701 phosphorylation of the resulting protein in response to stimulation with IFN-α or IFN-γ (Figure 2B). Both Y701C and L706S STAT1 proteins impaired phosphorylation. As previously reported, the

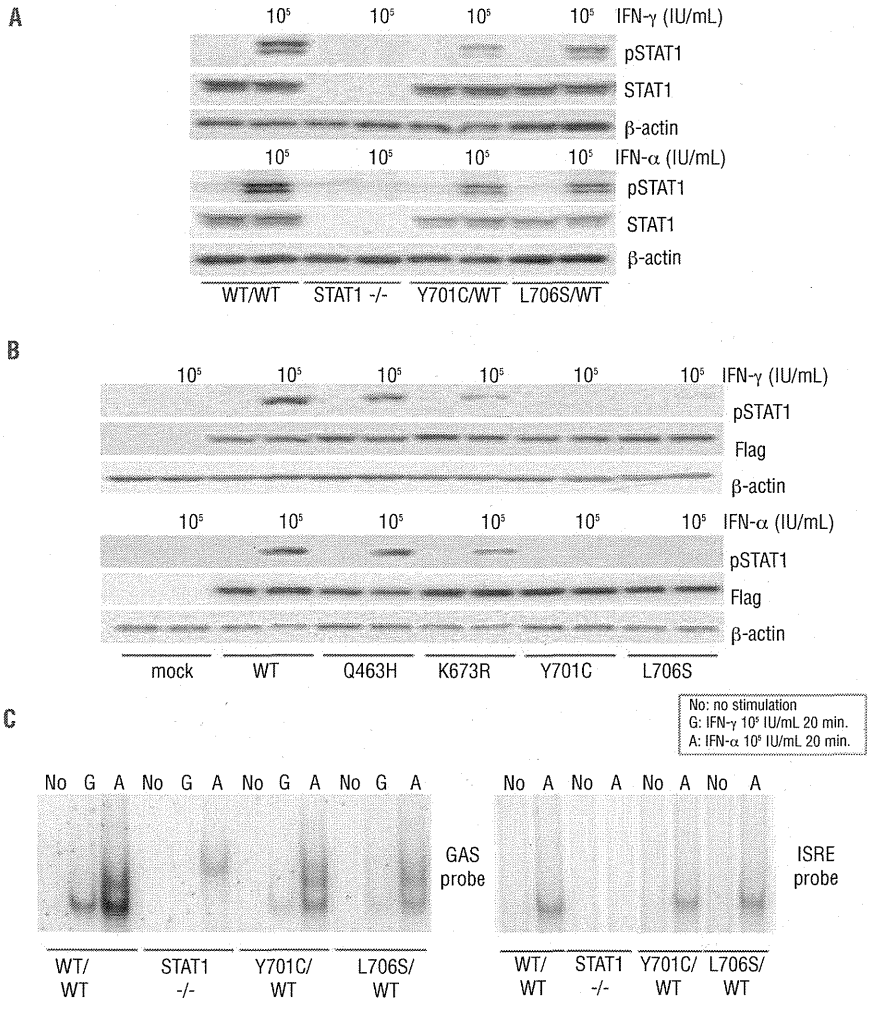

Figure 2. **STAT1 phosphorylation and DNA-binding ability in EBV-B cells. STAT1 production and phosphorylation in EBV-B cells (A) and transiently transfected U3C cells (B). The cells were stimulated with 10^5 IU/mL IFN for 15 min and subjected to immunoblot analysis. (A) EBV-B cells carrying heterozygous Y701C or L706S mutations showed a marked impairment of phosphorylation. The level of pSTAT1 was decreased in Y701C or L706S carrying cells by as much as 50.0% or 57.6% after IFN-γ stimulation and up to 66.3 % or 61.5 % after IFN-α stimulation when compared with healthy controls. (B) The Q463H STAT1 protein was normally phosphorylated, to levels similar to those observed for the WT protein. K673R STAT1 was only weakly phosphorylated. The Y701C STAT1 protein was not phosphorylated. (C) DNA-binding ability in EBV-B cells, as assessed by electrophoretic mobility shift assay with GAS and ISRE probes. EBV-B cells carrying Y701C or L706S mutations displayed a marked impairment of GAF DNA-binding ability. This impairment was particularly strong after IFN-γ stimulation. The ability of ISGF3 to bind DNA upon stimulation with IFN-α was preserved at almost normal levels in the patients' cells. At least two independent experiments were performed. (G: 10^5 IU/mL IFN-γ, A: 10^5 IU/mL IFN-α)**

phosphorylation of K673R STAT1 was partially impaired.[16] By contrast, the Q463H STAT1 mutant was phosphorylated to almost the same degree as the WT protein. We then analyzed the nuclear translocation of STAT1 in U2OS cells stably expressing flag-tagged WT, Q463H, K673R, L706S and Y701C STAT1 mutant alleles. Unphosphorylated STAT1 was mostly present in the cytoplasm before IFN-γ stimulation (*Online Supplementary Figure S2A*). After IFN-γ stimulation, STAT1 was found in the nucleus in cells producing the WT and Q463H STAT1 proteins (*Online Supplementary Figure S2B*). By contrast, STAT1 nuclear translocation was severely impaired in cells producing the Y701C and L706S STAT1 proteins. The K673R mutant STAT1 protein was present in both the nucleus and the cytoplasm, suggesting incomplete nuclear translocation. These results suggest that the Y701C mutation, like L706S, prevents STAT1 phosphorylation and nuclear translocation.

Comparison of the Y701C and L706S mutations

Both the Y701C and L706S mutations affect residues in the tail segment domain of STAT1. We focused on these two mutations and performed further functional characterization. We treated cells carrying these mutations with the tyrosine phosphatase inhibitor pervanadate and then analyzed the phosphorylation of STAT1 upon IFN-γ stimulation.[29] STAT1 phosphorylation was restored in the presence of pervanadate in cells carrying the L706S mutation, whereas no such restoration was observed for the Y701C mutant (Figure 3A). Conversely, pervanadate treatment did not rescue GAF-DNA binding for L706S STAT1 (Figure 3A). We investigated the mechanisms underlying these experimental observations by extracting the cytosol and investigating STAT1 phosphorylation by immunoblotting (Figure 3B). The L706S STAT1 protein showed almost normal levels of phosphorylation in the cytosol fraction after pervanadate treatment, whereas

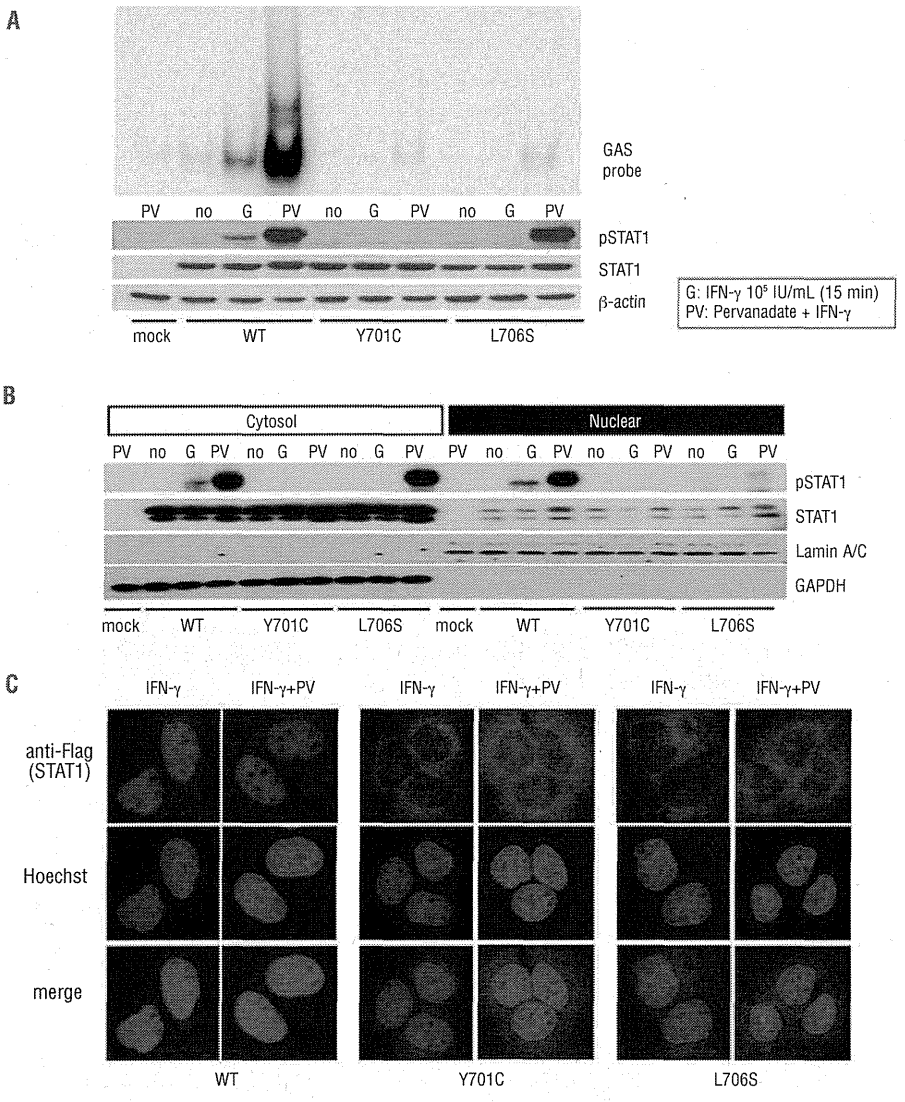

Figure 3. **Comparison of the Y701C and L706S mutations.** (A) **U3C transfectants were stimulated with 10^5 IU/mL IFN-γ in the presence or absence of pervanadate for 15 min and subjected to immunoblotting and electrophoretic mobility shift assay. The L706S STAT1 protein was phosphorylated to almost normal levels in response to IFN-γ stimulation in the presence of pervanadate, whereas no phosphorylation of the Y701C STAT1 protein was observed. However, L706S STAT1 was still associated with a lack of GAF-DNA binding, even after its phosphorylation had been restored.** (B) **STAT1 phosphorylation was investigated in the nuclear and cytosolic fractions, by immunoblotting. The phosphorylated L706S STAT1 protein was mostly present in the cytosol fraction.** (C) **U2OS cells stably expressing Flag-tagged WT, Y701C, or L706S STAT1 were stimulated with IFN-γ for 30 min in the presence or absence of pervanadate and subjected to immunostaining. Nuclear translocation was severely impaired in cells producing either Y701C or L706S STAT1, even after pervanadate treatment. At least two independent experiments were carried out.**

phosphorylation was severely impaired in the nuclear fraction. These results suggest that the L706S mutation impairs both phosphorylation and nuclear translocation. This impairment of the nuclear translocation of L706S STAT1 was confirmed by immunostaining (Figure 3C). The L706S mutant protein was, therefore, considered to have at least two molecular defects: severe impairments of both phosphorylation and the nuclear translocation of STAT1. By contrast, Y701C STAT1 phosphorylation was totally abolished and could not be restored by pervanadate treatment.

Transcriptional activity of the mutant STAT1 proteins

We investigated the impact of the STAT1 Y701C mutation on the transcriptional activities of GAS and ISRE, by carrying out reporter assays with GAS or ISRE reporter plasmids. Production of the Y701C and L706S STAT1 proteins was associated with abolition of the transcriptional activities of both GAS and ISRE (*Online Supplementary Figure S3A,C*). Co-transfection experiments revealed that these mutant proteins had negative effects on the WT protein in GAS transcriptional activity (*Online Supplementary Figure S3B*). Furthermore, a dose-dependent negative-dominance effect was clearly observed for the Y701C and L706S mutant proteins. By contrast, ISRE transcriptional activity remained at almost normal levels in cells co-transfected with the L706S plasmid (*Online Supplementary Figure S3D*). The level of ISRE transcriptional activity was repeatedly found to be lower with Y701C STAT1, but no clear dominant-negative effect was detected. These results are consistent with the results we observed in an electrophoretic mobility shift assay using EBV-B cells. Thus, the Y701C STAT1 allele has a dominant-negative effect, decreasing GAS activation but not ISRE activation.

Downstream gene induction in CD14-positive monocytes and Epstein-Barr virus-B cells

The induction of downstream interferon-stimulated genes (ISG) has been investigated with EBV-B cells from patients and in gene expression experiments using U3C cells.[15] We investigated the impact of the Y701C mutation further, by studying the induction of ISG in CD14-positive monocytes from patients, comparing the results obtained with those for EBV-B cells. We first purified CD14-positive monocytes, stimulated them with IFN-γ and analyzed the expression of the downstream ISG encoding *CXCL9* and *IRF1*, by real-time quantitative PCR analysis. Strong induction of *CXCL9* was observed at late time points (6 hours) in healthy controls, but this induction was severely impaired in the patients' cells (Figure 4A). In contrast, IRF1 induction was observed at both early and late time points. The patients' cells displayed a mild but significant impairment of *IRF1* induction at late time points, whereas the difference observed at early time points was not statistically significant. We then investigated the induction of *CXCL9*, *IRF1* and *ISG15* in EBV-B cells. The induction of these three ISG was STAT1-dependent, as shown by the abolition of induction in STAT1-null EBV-B cells. EBV-B cells carrying heterozygous Y701C or L706S mutations displayed severely impaired induction of *CXCL9* and *ISG15* in response to interferons (Figure 4B,C). Unlike CD14-positive monocytes, the peak of *IRF1* induction was observed at early time points in EBV-B cells. The impairment of *IRF1* induction was mild and mostly observed at early time points in EBV-B cells from the patients. Thus, CD14-positive monocytes and EBV-B cells behaved similarly, but not identically, in terms of ISG induction in response to IFN-γ stimulation. These results suggest that the induction of ISG is impaired in the patients' cells.

Discussion

We report here a novel heterozygous *STAT1* mutation, 2102 A>G (Y701C), which results in STAT1 deficiency and AD MSMD. The Y701 residue serves as a site of phosphorylation for STAT1, this phosphorylation playing a key role in STAT1-mediated signal transduction. Indeed, AD *STAT1* mutations impairing STAT1 phosphorylation have been shown to underlie the pathogenesis of MSMD.[14-17] Furthermore, AD mutations that cause gains of phosphorylation because they impair the nuclear dephosphorylation of STAT1 have been identified in patients with chronic mucocutaneous candidiasis.[30-34] The Y701C mutant STAT1 protein displayed a complete abolition of Y701 phosphorylation and downstream events, such as the nuclear translocation and transcriptional activities of GAS and ISRE. The Y701C *STAT1* allele is dominant for GAF, but recessive for ISGF3. This observation is highly consistent with previously identified STAT1 mutations in patients with AD STAT1 deficiencies and the molecular mechanisms can be explained by differences in the structure of GAS (homodimer of STAT1) and ISGF3 (heterodimer of STAT1/STAT2/IRF9).[14-17] The Y701C mutation is thus responsible for MSMD without viral disease. Two heterozygous *STAT1* mutations, Y701C and L706S, affect residues located in the same tail segment domain and result in the impairment of Y701 phosphorylation. However, these two mutants responded differently to stimulation in the presence of pervanadate. This treatment rescued Y701 phosphorylation in L706S STAT1, but not in the Y701C protein. The functional defect seemed to be more severe for the Y701C than for the L706S mutant protein, as shown by GAS reporter assays and real-time quantitative PCR analysis. The Y701C mutation may therefore have a stronger negative impact *in vitro* than L706S *STAT1*. However, in contrast to the findings of these *in vitro* studies, the clinical symptoms of the patient and his mother were similar to those of previously identified patients with AD STAT1 deficiency.

We also investigated the induction of ISG upon IFN-γ stimulation in CD14-positive monocytes from the patients. ISG induction has been intensively investigated in EBV-B cells,[15,17] but this is the first study to investigate the induction of ISG in primary cells from patients. Both EBV-B cell lines and primary monocytes from the patients showed severe impairment of *CXCL9* induction. Minor differences in induction patterns were observed, but both types of cell showed mild impairment of *IRF1* induction. Thus, the impairment of ISG induction was confirmed not only in EBV-B cells, but also in the patients' monocytes. IL-12p40 induction is totally dependent on Irf1 in mice.[35-37] Macrophages from *Irf1*-null mice display impaired induction of inducible nitric oxide synthase in response to lipopolysaccharide.[38,39] Furthermore, *Irf1*-null mice develop severe symptoms when infected with *Mycobacterium bovis*. Thus, the impairment of *IRF1* induction observed in CD14-positive monocytes may contribute to host susceptibility to mycobacteria. We also observed an impairment in *ISG15* induction in the patients' EBV-B cells. The recent

identification of ISG15 deficiency in some human patients with MSMD has provided evidence of an important role for this molecule in host immunity to mycobacteria.[11] Heterozygous *STAT1* mutations thus have negative effects on the downstream induction of ISG involved in host defense against mycobacteria, and this *in vitro* cellular phenotype is commonly observed in the patients' cells. However, the magnitude of this negative impact may dif-

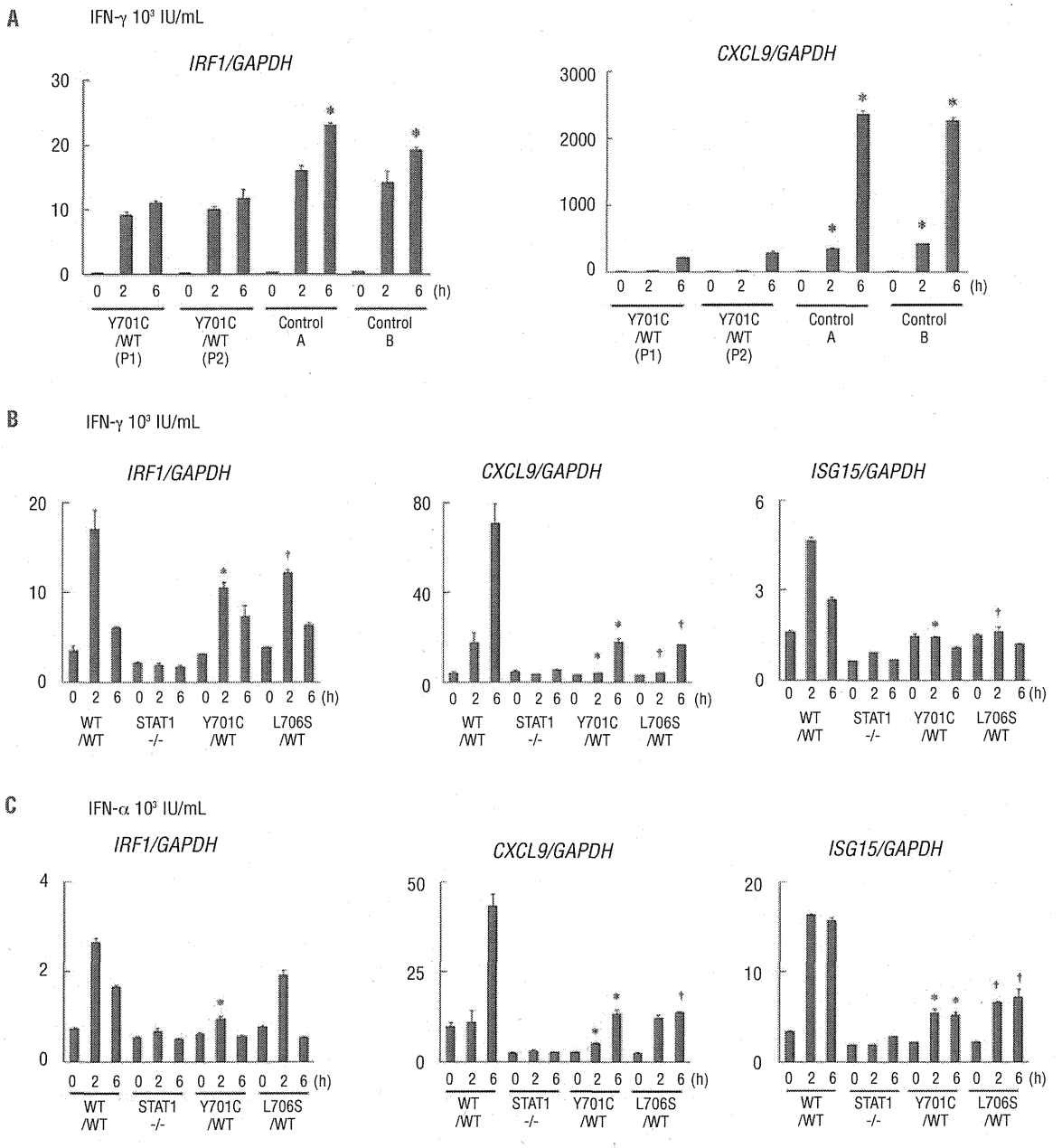

Figure 4. Analysis of gene expression. The induction of ISG was analyzed by real-time quantitative PCR. (A) CD14-positive monocytes from the patients (P1, P2) and two healthy controls were stimulated with 10^3 IU/mL IFN-γ (for 2 or 6 h) and the induction of *CXCL9* and *IRF1* was investigated. The induction of *CXCL9* was severely impaired in the patients' cells, whereas the induction of *IRF1* was only mildly impaired. *Differences were statistically significant in monocytes from the patients compared with those from healthy individuals ($P<0.05$). (B, C) The induction of *CXCL9*, *IRF1* and *ISG15* in EBV-B cells from the patients, Y701C/WT and L706S/WT cells, and cells from healthy individuals, in response to IFN-γ (B) or IFN-α (C) stimulation. EBV-B cells carrying Y701C or L706S mutations displayed severe impairment of *CXCL9* induction in response to IFN stimulation. The induction of *IRF1* and *ISG15* was also impaired, but to a lesser extent than that of *CXCL9*. ISG expression was normalized with respect to *GAPDH*. The results shown are representative of three independent experiments, except for the CD14⁺ monocyte experiment (which was performed twice). Differences were statistically significant between cells carrying either the Y701C mutation *($P<0.05$) or L706S mutation †($P<0.05$) and EBV-B cells from healthy individuals.

fer between cell types and between the ISG induced. The induction of ISG has also been intensively investigated in patients with AR STAT1 deficiency.[22] As in the current study, the severity of impairment differed in the patient's cells depending on the ISG induced. These observations reflect the complexity of STAT1-mediated signaling.[40]

Including the two patients studied here, 11 patients with AD STAT1 deficiency have been identified to date. Five of these 11 patients have developed multifocal osteomyelitis, a typical clinical feature of patients with AD partial IFN-γR1 deficiency.[4,41] Our initial patient had multifocal osteomyelitis showing tuberculoid granulomas without the detection of pathogenic mycobacterium by culture and/or PCR amplification. Additionally, his mother had a history of multifocal osteomyelitis. These observations emphasize the importance of multifocal osteomyelitis as one of the representative clinical manifestation even in patients with AD STAT1 deficiency. We have summarized the clinical manifestations of 11 patients with AD STAT1 deficiency,[14-17] 53 patients with AD partial IFN-γR1 deficiency,[41-45] 14 patients with AR partial IFN-γR1 deficiency[46] and 102 patients with AR IL-12Rβ1 deficiency,[47] the most common genetic etiology of MSMD (Table 1). The frequency of multifocal osteomyelitis was high in AD STAT1 deficiency (45.5%), AD partial IFN-γR1 deficiency (79.2%) and AR partial IFN-γR1 deficiency (50.0%), but lower in patients with AR complete IFN-γR1 deficiency (13%).[41] Unfortunately, this clinical manifestation has not been investigated in patients with AR IL-12Rβ1 deficiency.[47] In many cases, either BCG or environmental mycobacteria have been proven to be present by biopsy of osteomyelitis. By contrast, the frequency of BCG disease, a common sign in patients with MSMD, in patients vaccinated with BCG is similar to that in AD STAT1 deficiency (77.8%), AD partial IFN-γR1 deficiency (76.7%), AR partial IFN-γR1 deficiency (85.7%) and AR IL-12Rβ1 deficiency (77.9%). The clinical signs of AD STAT1 deficiency may, therefore, be considered to be similar to those of partial IFN-γR1 deficiency. There are several possible reasons for this: (i) STAT1 is a non-redundant downstream transcription factor for IFN-γ signaling;[4] (ii) STAT1 mutations impair GAF-mediated signaling, but not ISGF3-mediated signaling, and IFN-γ induces GAF, but not ISGF3;[48] (iii) IFN-γ signaling is only partially impaired in both disorders.[4] The clinical similarities between these two disorders support our hypothesis that the symptoms accompanying AD STAT1 deficiency result from an impairment of cellular responses to IFN-γ. Multifocal osteomyelitis is a characteristic symptom common to three different disorders: AD partial IFN-γR1 deficiency, AR partial IFN-γR1 deficiency and AD STAT1 deficiency. Multifocal osteomyelitis should, therefore, lead to investigations of both STAT1 and IFN-γR1.

Table 1. **Comparison of clinical manifestations.**

	AD STAT1 deficiency	AD partial IFN-γR1 deficiency	AR partial IFN-γR1 deficiency	AR IL-12Rβ1 deficiency
N. of cases	11	53	14	102
Onset of MSMD	5.3y (0.5y-18y)	10.8y (0.1y-62y)	11.2y (0.1y-31y)	2.4y (0.1y-31y)
BCG disease (among vaccinated patients)	7/9	23/30	6/7	67/86
Environmental mycobacteria	5/11	42/53	6/14	19/102
M. tuberculosis complex		2/53	1/14	5/102
Salmonella spp.	none	2/53	3/14	44/102
Severe viral infection	none	1/53	none	none
Osteomyelitis	5/11	42/53	7/14	
Locations of mycobacterial infections				
Nodes	2/11	30/53		6/14
Other organs	4/11	11/53		6/14
References	*14-17*	*41-45*	*46*	*47*

Acknowledgments

The authors would like to thank Xiao-Fei Kong, MD, PhD, Vanessa Bryant, PhD, Dusan Bogunovic, PhD, Alexandra Kreins, MD, Marcela Moncada-Velez, BSc, Michael Ciancaneli, PhD, and Avinash Abhyankar, MD, PhD, for helpful discussions and critical reading. We also thank the members of the laboratory, Yelena Nemirovskaya and Eric Anderson for secretarial assistance, and Tiffany Nivare for technical assistance. Sequence analysis support was provided by the Analysis Center of Life Science, Natural Science Center for Basic Research and Development, Hiroshima University.

Funding

This study was supported, in part, by Grants in Aid for Scientific Research from the Japan Society for the Promotion of Science [22591161 to M.K.], and by Research on Measures for Intractable Diseases funding from the Japanese Ministry of Health, Labor and Welfare [H22-Nanchi-ippan-078 to MK]. This study was also supported, in part, by the Rockefeller University and grants from the National Center for Research Resources, and the National Center for Advancing Sciences (NCATS), National Institutes of Health (NIH) grant number 8UL1TR000043, NIH grant number R01AI089970, and the St. Giles Foundation. SC was supported by the AXA Research Fund and X-FK by the Stony Wold-Herbert Fund.

Authorship and Disclosures

Information on authorship, contributions, and financial & other disclosures was provided by the authors and is available with the online version of this article at www.haematologica.org.

References

1. Casanova JL, Abel L. Genetic dissection of immunity to mycobacteria: the human model. Annu Rev Immunol. 2002;20:581-620.
2. Hamosh A, Scott AF, Amberger JS, Bocchini CA, McKusick VA. Online Mendelian Inheritance in Man (OMIM), a knowledgebase of human genes and genetic disorders. Nucleic Acids Res. 2005;33(Database issue):D514-7.
3. Alcais A, Fieschi C, Abel L, Casanova JL. Tuberculosis in children and adults: two distinct genetic diseases. J Exp Med. 2005;202(12):1617-21.
4. Filipe-Santos O, Bustamante J, Chapgier A, Vogt G, de Beaucoudrey L, Feinberg J, et al. Inborn errors of IL-12/23- and IFN-gamma-mediated immunity: molecular, cellular, and clinical features. Semin Immunol. 2006;18(6):347-61.
5. Vogt G, Bustamante J, Chapgier A, Feinberg J, Boisson Dupuis S, Picard C, et al. Complementation of a pathogenic IFNGR2 misfolding mutation with modifiers of N-glycosylation. J Exp Med. 2008;205(8):1729-37.
6. Bustamante J, Arias AA, Vogt G, Picard C,

Galicia LB, Prando C, et al. Germline CYBB mutations that selectively affect macrophages in kindreds with X-linked predisposition to tuberculous mycobacterial disease. Nat Immunol. 2011;12(3):213-21.
7. Hambleton S, Salem S, Bustamante J, Bigley V, Boisson-Dupuis S, Azevedo J, et al. IRF8 mutations and human dendritic-cell immunodeficiency. N Engl J Med. 2011;365(2):127-38.
8. Al-Muhsen S, Casanova JL. The genetic heterogeneity of mendelian susceptibility to mycobacterial diseases. J Allergy Clin Immunol. 2008;122(6):1043-51; quiz 52-3.
9. Boisson-Dupuis S, Kong XF, Okada S, Cypowyj S, Puel A, Abel L, et al. Inborn errors of human STAT1: allelic heterogeneity governs the diversity of immunological and infectious phenotypes. Curr Opin Immunol. 2012;24(4):364-78.
10. Casanova JL, Holland SM, Notarangelo LD. Inborn errors of human JAKs and STATs. Immunity. 2012;36(4):515-28.
11. Bogunovic D, Byun M, Durfee LA, Abhyankar A, Sanal O, Mansouri D, et al. Mycobacterial disease and impaired IFN-gamma immunity in humans with inherited ISG15 deficiency. Science. 2012;337(6102):1684-8.
12. Casanova JL, Abel L. Inborn errors of immunity to infection: the rule rather than the exception. J Exp Med. 2005;202(2):197-201.
13. Alcais A, Quintana-Murci L, Thaler DS, Schurr E, Abel L, Casanova JL. Life-threatening infectious diseases of childhood: single-gene inborn errors of immunity? Ann NY Acad Sci. 2010;1214:18-33.
14. Dupuis S, Dargemont C, Fieschi C, Thomassin N, Rosenzweig S, Harris J, et al. Impairment of mycobacterial but not viral immunity by a germline human STAT1 mutation. Science. 2001;293(5528):300-3.
15. Chapgier A, Boisson-Dupuis S, Jouanguy E, Vogt G, Feinberg J, Prochnicka-Chalufour A, et al. Novel STAT1 alleles in otherwise healthy patients with mycobacterial disease. PLoS Genet. 2006;2(8):e131.
16. Tsumura M, Okada S, Sakai H, Yasunaga S, Ohtsubo M, Murata T, et al. Dominant-negative STAT1 SH2 domain mutations in unrelated patients with Mendelian susceptibility to mycobacterial disease. Hum Mutat. 2012;33(9):1377-87.
17. Sampaio EP, Bax HI, Hsu AP, Kristosturyan E, Pechacek J, Chandrasekaran P, et al. A novel STAT1 mutation associated with disseminated mycobacterial disease. J Clin Immunol. 2012;32(4):681-9.
18. Kristensen IA, Veirum JE, Moller BK, Christiansen M. Novel STAT1 alleles in a patient with impaired resistance to mycobacteria. J Clin Immunol. 2011;31(2):265-71.
19. Vairo D, Tassone L, Tabellini G, Tamassia N, Gasperini S, Bazzoni F, et al. Severe impairment of IFN-gamma and IFN-alpha responses in cells of a patient with a novel STAT1 splicing mutation. Blood. 2011;118(7):1806-17.
20. Dupuis S, Jouanguy E, Al-Hajjar S, Fieschi C, Al-Mohsen IZ, Al-Jumaah S, et al. Impaired response to interferon-alpha/beta and lethal viral disease in human STAT1 deficiency. Nat Genet. 2003;33(3):388-91.
21. Chapgier A, Wynn RF, Jouanguy E, Filipe-Santos O, Zhang S, Feinberg J, et al. Human complete Stat-1 deficiency is associated with defective type I and II IFN responses in vitro but immunity to some low virulence viruses in vivo. J Immunol. 2006;176(8):5078-83.
22. Kong XF, Ciancanelli M, Al-Hajjar S, Alsina L, Zumwalt T, Bustamante J, et al. A novel form of human STAT1 deficiency impairing early but not late responses to interferons. Blood. 2010;116(26):5895-906.
23. Shuai K, Ziemiecki A, Wilks AF, Harpur AG, Sadowski HB, Gilman MZ, et al. Polypeptide signalling to the nucleus through tyrosine phosphorylation of Jak and Stat proteins. Nature. 1993;366(6455):580-3.
24. Chen X, Vinkemeier U, Zhao Y, Jeruzalmi D, Darnell JE Jr, Kuriyan J. Crystal structure of a tyrosine phosphorylated STAT-1 dimer bound to DNA. Cell. 1998;93(5):827-39.
25. Bach EA, Aguet M, Schreiber RD. The IFN gamma receptor: a paradigm for cytokine receptor signaling. Annu Rev Immunol. 1997;15:563-91.
26. van Boxel-Dezaire AH, Stark GR. Cell type-specific signaling in response to interferon-gamma. Curr Top Microbiol Immunol. 2007;316:119-54.
27. Kong XF, Vogt G, Itan Y, Macura-Biegun A, Szaflarska A, Kowalczyk D, et al. Haploinsufficiency at the human IFNGR2 locus contributes to mycobacterial disease. Hum Mol Genet. 2013;22(4):769-81.
28. Bernabei P, Coccia EM, Rigamonti L, Bosticardo M, Forni G, Pestka S, et al. Interferon-gamma receptor 2 expression as the deciding factor in human T, B, and myeloid cell proliferation or death. J Leukoc Biol. 2001;70(6):950-60.
29. Tourkine N, Schindler C, Larose M, Houdebine LM. Activation of STAT factors by prolactin, interferon-gamma, growth hormones, and a tyrosine phosphatase inhibitor in rabbit primary mammary epithelial cells. J Biol Chem. 1995;270(36):20952-61.
30. Liu L, Okada S, Kong XF, Kreins AY, Cypowyj S, Abhyankar A, et al. Gain-of-function human STAT1 mutations impair IL-17 immunity and underlie chronic mucocutaneous candidiasis. J Exp Med. 2011;208(8):1635-48.
31. van de Veerdonk FL, Plantinga TS, Hoischen A, Smeekens SP, Joosten LA, Gilissen C, et al. STAT1 mutations in autosomal dominant chronic mucocutaneous candidiasis. N Engl J Med. 2011;365(1):54-61.
32. Smeekens SP, Plantinga TS, van de Veerdonk FL, Heinhuis B, Hoischen A, Joosten LA, et al. STAT1 hyperphosphorylation and defective IL12R/IL23R signaling underlie defective immunity in autosomal dominant chronic mucocutaneous candidiasis. PLoS One. 2011;6(12):e29248.
33. Takezaki S, Yamada M, Kato M, Park MJ, Maruyama K, Yamazaki Y, et al. Chronic mucocutaneous candidiasis caused by a gain-of-function mutation in the STAT1 DNA-binding domain. J Immunol. 2012;189(3):1521-6.
34. Toth B, Mehes L, Tasko S, Szalai Z, Tulassay Z, Cypowyj S, et al. Herpes in STAT1 gain-of-function mutation [corrected]. Lancet. 2012;379(9835):2500.
35. Taniguchi T, Ogasawara K, Takaoka A, Tanaka N. IRF family of transcription factors as regulators of host defense. Annu Rev Immunol. 2001;19:623-55.
36. Taki S, Sato T, Ogasawara K, Fukuda T, Sato M, Hida S, et al. Multistage regulation of Th1-type immune responses by the transcription factor IRF-1. Immunity. 1997;6(6):673-9.
37. Lohoff M, Ferrick D, Mittrucker HW, Duncan GS, Bischof S, Rollinghoff M, et al. Interferon regulatory factor-1 is required for a T helper 1 immune response in vivo. Immunity. 1997;6(6):681-9.
38. Kamijo R, Harada H, Matsuyama T, Bosland M, Gerecitano J, Shapiro D, et al. Requirement for transcription factor IRF-1 in NO synthase induction in macrophages. Science. 1994;263(5153):1612-5.
39. Martin E, Nathan C, Xie QW. Role of interferon regulatory factor 1 in induction of nitric oxide synthase. J Exp Med. 1994;180(3):977-84.
40. Gough DJ, Levy DE, Johnstone RW, Clarke CJ. IFNgamma signaling - does it mean JAK-STAT? Cytokine Growth Factor Rev. 2008;19(5-6):383-94.
41. Dorman SE, Picard C, Lammas D, Heyne K, van Dissel JT, Baretto R, et al. Clinical features of dominant and recessive interferon gamma receptor 1 deficiencies. Lancet. 2004;364(9451):2113-21.
42. Hoshina T, Takada H, Sasaki-Mihara Y, Kusuhara K, Ohshima K, Okada S, et al. Clinical and host genetic characteristics of mendelian susceptibility to mycobacterial diseases in Japan. J Clin Immunol. 2011;31(3):309-14.
43. Lee WI, Huang JL, Lin TY, Hsueh C, Wong AM, Hsieh MY, et al. Chinese patients with defective IL-12/23-interferon-gamma circuit in Taiwan: partial dominant interferon-gamma receptor 1 mutation presenting as cutaneous granuloma and IL-12 receptor beta1 mutation as pneumatocele. J Clin Immunol. 2009;29(2):238-45.
44. Glosli H, Stray-Pedersen A, Brun AC, Holtmon LW, Tonjum T, Chapgier A, et al. Infections due to various atypical mycobacteria in a Norwegian multiplex family with dominant interferon-gamma receptor deficiency. Clin Infect Dis. 2008;46(3):e23-7.
45. Okada S, Ishikawa N, Shirao K, Kawaguchi H, Tsumura M, Ohno Y, et al. The novel IFNGR1 mutation 774del4 produces a truncated form of interferon-gamma receptor 1 and has a dominant-negative effect on interferon-gamma signal transduction. J Med Genet. 2007;44(8):485-91.
46. Sologuren I, Boisson-Dupuis S, Pestano J, Vincent QB, Fernandez-Perez L, Chapgier A, et al. Partial recessive IFN-{gamma}R1 deficiency: genetic, immunological and clinical features of 14 patients from 11 kindreds. Hum Mol Genet. 2011;20(8):1509-23.
47. de Beaucoudrey L, Samarina A, Bustamante J, Cobat A, Boisson-Dupuis S, Feinberg J, et al. Revisiting human IL-12Rbeta1 deficiency: a survey of 141 patients from 30 countries. Medicine (Baltimore). 2010;89(6):381-402.
48. Ginter T, Bier C, Knauer SK, Sughra K, Hildebrand D, Munz T, et al. Histone deacetylase inhibitors block IFNgamma-induced STAT1 phosphorylation. Cell Signal. 2012;24(7):1453-60.

bjh research paper

Identification of the integrin β3 L718P mutation in a pedigree with autosomal dominant thrombocytopenia with anisocytosis

Yoshiyuki Kobayashi,[1,2] Hirotaka Matsui,[1]* Akinori Kanai,[1] Miyuki Tsumura,[2] Satoshi Okada,[2] Mizuka Miki,[2] Kazuhiro Nakamura,[2] Shinji Kunishima,[3] Toshiya Inaba[1] and Masao Kobayashi[2]

[1]Department of Molecular Oncology and Leukaemia Programme Project, Research Institute for Radiation Biology and Medicine, Hiroshima University, [2]Department of Paediatrics, Graduate School of Biomedical and Health Sciences, Hiroshima University, Minami-ku, Hiroshima, and [3]Department of Advanced Diagnosis, Clinical Research Centre, National Hospital Organization Nagoya Medical Centre, Nagoya, Aichi, Japan

Received 29 June 2012; accepted for publication 22 October 2012

Correspondence: Hirotaka Matsui, Department of Molecular Oncology and Leukemia Program Project, Research Institute for Radiation Biology and Medicine, Hiroshima University, 1-2-3 Kasumi, Minami-ku, Hiroshima 734-8553, Japan.
E-mail: hmatsui@hiroshima-u.ac.jp

Summary

αIIbβ3 integrin mutations that result in the complete loss of expression of this molecule on the platelet surface cause Glanzmann thrombasthenia. This is usually autosomal recessive, while other mutations are known to cause dominantly inherited macrothrombocytopenia (although such cases are rare). Here, we report a 4-generation pedigree including 10 individuals affected by dominantly inherited thrombocytopenia with anisocytosis. Six individuals, whose detailed clinical and laboratory data were available, carried a non-synonymous *ITGB3* gene alteration resulting in mutated integrin β3 (ITGB3)-L718P. This mutation causes partial activation of the αIIbβ3 complex, which promotes the generation of abnormal pro-platelet-like protrusions through downregulating RhoA (RHOA) activity in transfected Chinese Hamster Ovary cells. These findings suggest a model whereby the integrin β3-L718P mutation contributes to thrombocytopenia through gain-of-function mechanisms.

Keywords: integrin β3 L718P mutation, familial thrombocytopenia, autosomal dominant inheritance, whole exome sequencing, inhibition of RhoA.

Lifelong haemorrhagic syndromes are in part caused by point mutations in the *ITGA2B* and *ITGB3* genes encoding ITGA2B and ITGB3 proteins (integrin αIIb and β3, respectively). The αIIbβ3 complex regulates thrombopoiesis by megakaryocytes and aggregation of platelets in response to extracellular stimuli, such as ADP and collagen. The autosomal recessive syndrome, Glanzmann thrombasthenia, is the most frequently encountered disease caused by αIIbβ3 mutations (George *et al*, 1990; Nurden, 2006; Nurden & Nurden, 2008; Nurden *et al*, 2011a). Patients have a homozygous or a compound heterozygous mutation in the *ITGA2B* or *ITGB3* genes that causes loss of function of the αIIbβ3 complex. Although platelet counts and size are generally normal, patients typically have severe mucocutaneous bleeding, such as epistaxis, menorrhagia and gastrointestinal bleeding, frequently because of defects in platelet aggregation.

Mutations of the αIIbβ3 complex are also involved in congenital haemorrhagic diseases other than Glanzmann thrombasthenia (Ghevaert *et al*, 2008; Schaffner-Reckinger *et al*, 2009; Jayo *et al*, 2010; Kunishima *et al*, 2011; Nurden *et al*, 2011b). For example, the integrin β3 D723H mutation is found in autosomal dominant macrothrombocytopenia (Ghevaert *et al*, 2008). Biochemical analysis revealed that integrin β3-D723H is a gain of function mutation which activates the αIIbβ3 complex constitutively, albeit only partially. This results in the formation of proplatelet-like protrusions in transfected Chinese Hamster Ovary (CHO) cells, a model of relevance for the formation of macrothrombocytes (Ghevaert *et al*, 2008; Schaffner-Reckinger *et al*, 2009).

More recently, a sporadic patient carrying an integrin β3-L718P mutation was reported (Jayo *et al*, 2010). She had mild thrombocytopenia (127×10^9/l), platelet anisocytosis and reduced platelet aggregation potential. This mutation also induces abnormal proplatelet formation.

In the present study, we report a pedigree with a total 10 of individuals affected by a dominantly inherited haemorrhagic

First published online 17 December 2012
doi:10.1111/bjh.12160

syndrome. Six individuals whose detailed clinical and laboratory data are available, presented with thrombocytopenia accompanied by anisocytosis and carry a non-synonymous *ITGB3* T2231C alteration resulting in the integrin β3-L718P mutation. We also performed entire exon sequencing by a next-generation sequencing and found that the integrin β3-L718P mutation is most likely the sole gene responsible for thrombocytopenia in this pedigree.

Materials and methods

Written informed consent was obtained from individuals in the family in accordance with the Declaration of Helsinki for blood sampling and analysis undertaken with the approval of the Hiroshima University Institutional Review Board.

Patient

The patient was 4-year-old Japanese girl (iv.3 in Fig 1A), who presented with mild bleeding tendencies, such as recurrent nasal bleeding and purpura in her extremities. Her platelet count was 49–72 × 10^9/l with a mean platelet volume (MPV) of 9·8–10·9 fl. White blood cell and red blood cell counts were within the normal range and there were no morphological abnormalities including inclusions in neutrophils. Bone marrow examination was not performed. A total of six of her relatives, namely her father (iii.2), sister and brother (iv.1 and iv.2), two cousins (iv.4 and iv.5) and an aunt (iii.5), were subsequently found to have low platelet counts and were referred to our institute for further investigation.

Antibodies and reagents

Unconjugated or phycoerythrin-cyanin 5 (PC5)-conjugated anti-CD41 monoclonal antibody (Ab) (clone P2) against the αIIbβ3 complex (Beckman Coulter, Brea, CA, USA), fluorescein isothiocyanate (FITC)-conjugated anti-CD41a monoclonal Ab (clone HIP8) (Beckman Coulter), FITC- or peridinin chlorophyll (PerCP)-conjugated anti-CD61 monoclonal Ab (clone RUU-PL 7F12) (BD Biosciences, San Jose, CA, USA), FITC-conjugated PAC-1 (BD Biosciences) and Alexa488-conjugated human fibrinogen (Life Technologies, Carlsbad, CA, USA) were used in flow cytometry. Anti-CD61 monoclonal Ab (clone EP2417Y) (Abcam, Cambridge, UK), anti-DDDDK-tag polyclonal Ab (Medical & Biological Laboratories, Nagoya, Japan), Alexa488-conjugated phalloidin and Hoechst 33342 (both Life Technologies) were used for immunofluorescence microscopy. The oligopeptide Arg-Gly-Asp-Ser (RGDS) (Sigma–Aldrich, St Louis, MO, USA) was used to competitively inhibit the binding of ligands to αIIbβ3, and adenosine diphosphate (ADP) (nacalai tesque, Kyoto, Japan) was used for the stimulation of αIIbβ3 on platelets.

Construction and transfection of expression vectors

Full-length wild type (WT) *ITGA2B* and *ITGB3* cDNA were amplified by polymerase chain reaction (PCR) and cloned into pcDNA3·1 expression vectors. A PCR-mediated site-directed mutagenesis technique was applied to produce *ITGB3* mutants encoding integrin β3-L718P, -D723H and -T562N with or without truncation at the C-terminal side of Y^{759} (del. 759). *RHOA* cDNA, which encodes RhoA (RHOA) protein, was amplified by PCR and its mutants (T19N and Q63L) were generated by site-directed mutagenesis, followed by cloning into p3xFLAG-CMV-10 vectors (Sigma–Aldrich). The *ITGA2B* and *ITGB3* expression vectors were simultaneously transfected into CHO cells cultured in Ham's F12 medium supplemented with 10% fetal bovine serum at 37°C, in 5% CO_2, using Lipofectamine LTX reagent (Life Technologies) according to the manufacturer's instructions.

Immunofluorescent laser-scanning confocal microscopy

Cells grown on coverslips coated with 100 μg/ml fibrinogen were fixed with 4% paraformaldehyde, followed by permeabilization with phosphate-buffered saline containing 0·1% Triton X100. After blocking, the cells were stained with primary antibodies at appropriate dilutions, followed by staining with Alexa488- or Cy3-conjugated secondary antibodies together with Hoechst 33342. High-resolution immunofluorescent images were taken under a laser-scanning confocal microscopy (LSM5 Pascal, Carl Zeiss, Oberkochen, Germany) using a x63 objective.

Flow cytometry

The expression and activation of integrin αIIb and β3 on the platelet surface was indirectly estimated by flow cytometry with the antibodies described above. Mean fluorescence intensity (MFI) of values in an affected individual were divided by those in an unrelated normal control and recorded as relative MFI value (%). For the quantitative determination of αIIbβ3 molecules on the platelet surface, QIFIKIT (Dako, Glostrup, Denmark) was used according to the manufacturer's instructions. MFI of the calibration beads containing five populations (antibody-binding capacity: 2600, 9900, 46 000, 221 000 and 741 000) were 16·12, 63·83, 262·84, 1483·2 and 3772·1, respectively, whereas that of the negative control sample was 1·62. Therefore, αIIbβ3 molecules (copies/platelet) was calculated as $10^{(1.022 \times \log(\mathrm{MFI}) + 2.1679)} - 241$. Activation of platelets and CHO cells was estimated by methods previously described (Shattil *et al*, 1987; Hughes *et al*, 1996). Activation index was defined as $(F-F_0) / (F'-F_0)$, where F is the MFI of PAC-1-stained CHO cells transfected with αIIbβ3-L718P or αIIbβ3-D723H, and F_0 and F' are those transfected with αIIbβ3-WT and αIIbβ3-T562N, respectively. The samples were analyzed on a FACS Calibur (Becton Dickinson, Franklin Lakes, NJ, USA), equipped with an argon laser operating at 488 nm.

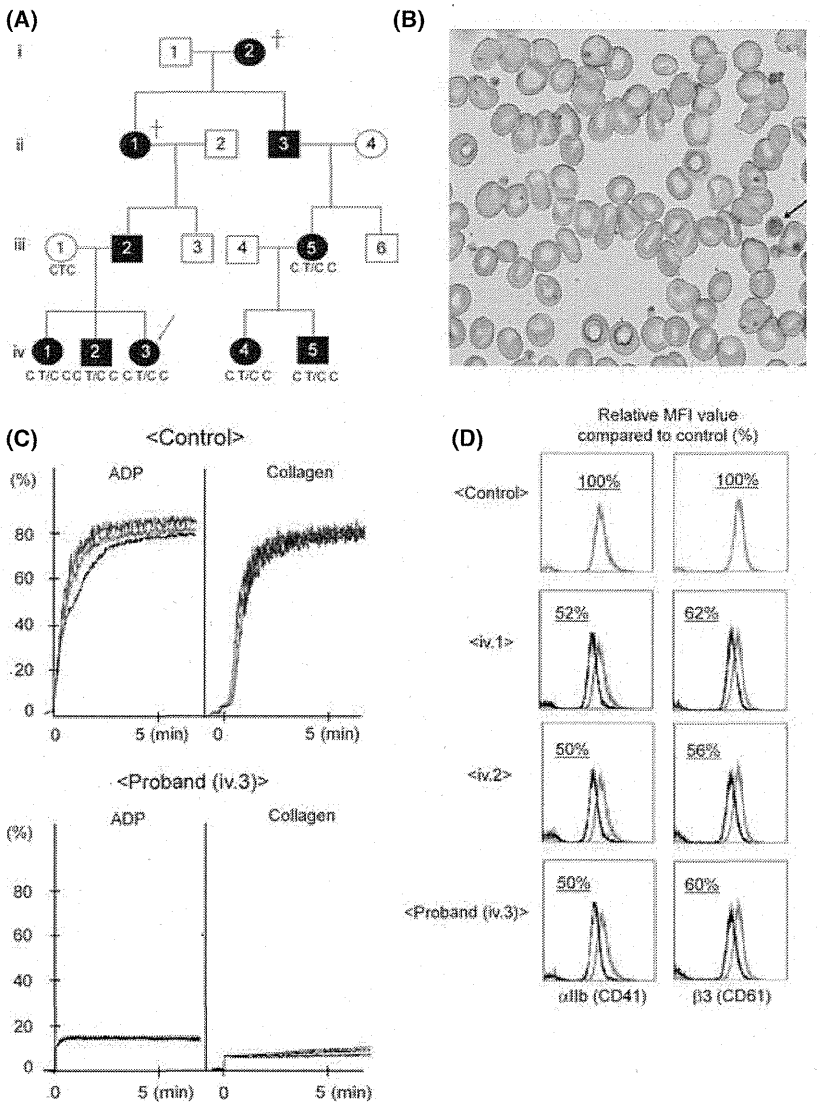

Fig 1. Platelet morphology and aggregation tracings. (A) The pedigree shows affected (filled) and unaffected (open) females (circles) and males (squares). The patient is indicated by an arrow. (B) Platelet morphology as determined by optical microscopy. Peripheral blood specimen obtained from the patient stained with May-Giemsa. The arrow indicates a macrothrombocyte. Original magnification × 600. (C) Representative platelet aggregation tracings in response to ADP and collagen stimuli in platelet-rich plasma from the patient and an unrelated normal control. (D) Flow cytometry of surface integrin αIIb (CD41) and β3 (CD61) expression. Samples were obtained from three affected individuals of the pedigree and an unrelated normal control. Data were calculated as relative MFI value (%), where MFIs of affected individuals were divided by MFI of a control sample.

Exome sequencing

Genomic DNA was obtained from four affected individuals in the pedigree and whole exome sequencing was performed. Briefly, 3 μg genomic DNA was fragmented by Covaris S2 (Covaris, Woburn, MA, USA) and ligated to adaptors, followed by hybridization to biotinylated RNA baits according to the manufacturer's instruction (Agilent Technologies, Santa Clara, CA, USA). The generated sequence tags were sequenced by the 76 bp paired-end protocol of Illumina GAIIx (Illumina, San Diego, CA, USA) and mapped onto the human genomic sequence (hg18, UCSC Genome Browser) using the sequence alignment program Eland (Illumina). Unmapped or redundantly mapped sequences were removed from the data set, and only uniquely mapped sequences were used for further analyses. Positions relative to RefSeq genes were calculated based on the respective genomic coordinates. Genomic coordinates of exons and the protein-coding regions of the RefSeq transcripts are as described in hg18. To verify the presence of *ITGB3* gene alteration, amplification and direct sequencing of a part of exon 14 was performed with the following primers; 5′-CATAGCCAGTTCAAGTGACTCCTG-3′ for forward primer and 5′-ACGATGGTACTGGCTGAACATGAC-3′ for reverse primer.

Results

Pedigree of a family with autosomal dominant thrombocytopenia with anisocytosis

In the original patient, marked platelet anisocytosis was observed in peripheral blood samples (Fig 1B). Platelet aggregation induced by ADP (1–4 μmol/l) and collagen (0·5–2 μg/ml) was markedly reduced (Fig. 1C and Table I), but agglutination induced by ristocetin (1·25 mg/ml) was within

the normal range (data not shown). Three affected individuals (iii.5, iv.1, and iv.2) showed abnormalities in platelet function similar to those of the original patient. In these affected individuals, the αIIb and β3 expression levels, which were indirectly estimated as relative MFI value (%), were 43–75% of a healthy control (Fig 1D and Table I). The number of αIIbβ3 molecules on the platelet surface in patients, as evaluated by flow cytometry using QIFIKIT, was 35 000–38 400 copies/platelet (MFI: 212·1 –232·4), whereas in an unaffected individual of the pedigree (iii.1) and an unrelated control, there were 65 200 and 62 100 copies/platelet (MFI: 389·2 and 371·3), respectively (Table I). The tendency to bleed was mild to moderate, as exemplified by the following episodes: when family member iv.1 received a bruise to the face, treatment with recombinant Factor VIIa was required because of persistent epistaxis; also, family member iii.5 had had to give birth by Caesarean section because of low platelet count. The family pedigree (Fig 1A), which shows no evidence of consanguineous marriage, strongly suggests the inheritance of thrombocytopenia as an autosomal dominant trait. The laboratory findings are shown in Table I.

Identification of the integrin β3 L718P mutation by whole exome analysis

To isolate a candidate gene alteration responsible for the thrombocytopenia, whole exome sequencing analysis was performed using genomic DNA obtained from the patient (iv.3), her sister and brother (iv.1 and iv.2) and a cousin (iv.4). A total of 794 non-synonymous gene alterations among 1551 SNPs that are not registered in dbSNP 129/130 were detected in the patient. To isolate the responsible gene, we selected non-synonymous gene alterations shared by the four affected individuals as strong candidates. Among the 90 alterations commonly found in the affected individuals of the pedigree (individual numbers of SNPs/mutations are shown in Table II), we focused on the heterozygous non-synonymous T2231C alteration in exon 14 of the *ITGB3* gene, which results in the substitution of leucine at 718 for proline (L718P) in the integrin β3 protein. We selected this because it was recently reported as a candidate mutation responsible for thrombocytopenia (Jayo *et al*, 2010). The presence of the mutation in six affected individuals of the pedigree (iv.1, iv.2, iv.3, iv.4, iii.5 and iv.5) and its absence in an unaffected individual (iii.1) and an unrelated control was confirmed by a direct-sequencing (Fig 2). As far as we could determine, no other non-synonymous gene alterations previously reported to cause thrombocytopenia or defective platelet function were present in the affected individuals of the pedigree. In addition, the L718 residue in integrin β3 is well-conserved between species and amino acid substitution in this position is predicted by bioinformatic tools, including Polyphen and SIFT, to cause a significant change in protein structure and function (data not shown). These observations strongly suggest that the L718P mutation in integrin β3 is the responsible gene alteration that causes familial thrombocytopenia.

Constitutive but partial activation of the αIIbβ3 complex by β3-L718P

To elucidate the effects of the integrin β3-L718P mutation on the activation status of αIIbβ3 complexes in resting or ADP-activated platelets, fresh platelets were analysed by flow cytometry using PAC-1, a ligand-mimicking antibody that specifically recognizes the activated form of the αIIbβ3 complex (Shattil *et al*, 1987).

Resting control platelets from healthy individuals bound PAC-1 with a similar affinity to those treated with RGDS, a peptide which competitively inhibits the binding of ligands for

Table I. Laboratory data of seven individuals of the pedigree.

						Relative MFI value compared to control (%)		αIIbβ3 molecules		Platelet aggregation (%)	
Patient	Sex	Age (years)	Platelet count ($\times 10^9$/l)	MPV (fl)	PDW (%)	αIIb	β3	MFI	copies/platelet	ADP (4 μM)	collagen (2·0 μg/ml)
iii.1	F	37	210	10·2	12·1	110	111	389·2	65 200	NA	NA
iii.5	F	34	38–67	8·5–11·3	10·0–19·0	43	75	NA	NA	15	12
iv.1	F	11	30–43	7·8–11·2	9·7–16·3	52	62	232·4	38 400	16	8
iv.2	M	8	49–64	10·3–11·1	10·1–14·7	50	56	216·4	35 700	23	16
iv.3	F	6	49–72	9·8–10·9	11·1–13·3	50	60	212·1	35 000	12	8
iv.4	F	4	32–59	9·9–10·8	12·3–15·6	NA	NA	NA	NA	NA	NA
iv.5	M	2	28–50	8·9–9·0	18·0–18·4	49	51	NA	NA	NA	NA

MPV, mean platelet volume (normal range: 9·4–12·3 fl); PDW, platelet distribution width (normal range: 9·5–14·8 %); NA, not available. αIIbβ3 molecules (copies/platelet) were calculated as $10^{(1\cdot022 \times \log(\mathrm{MFI}) + 2\cdot1679)} - 241$ (see *Materials and methods*).

Table II. Number of SNPs/mutations detected by whole exome sequencing.

Case	iv.1	iv.2	iv.3	iv.4
SNP	21 531	21 697	20 413	20 113
Not in dbSNP 129 and 130	1 674	1 722	1 473	1 551
Non-synonymous alternations				
Homozygous	62	58	65	42
Heterozygous	800	815	667	752
Non-synonymous (common)	90			

αIIbβ3 complex such as fibrinogen and PAC-1 (Fig 3A, compare black and blue lines), indicating that wild-type αIIbβ3 in resting platelets is not activated. In contrast, platelets obtained from the affected individuals (iii.5, iv.1, iv.2 and iv.3) showed a slight increase of PAC-1 binding compared to those treated with RGDS (Fig 3A). Indeed, resting platelets from affected individuals showed a slight but significant increase of PAC-1 binding relative to healthy individuals (Fig 3A, top panel). In addition, flow cytometric analysis using FITC-conjugated fibrinogen also showed a significant increase of fibrinogen binding potential in resting platelets from affected individuals compared with healthy controls (bottom panel). Because MPV (shown in Table I) did not exceed the normal range (9·4–12·3 fl) and surface expression levels of αIIbβ3 were lower in patients than controls (Fig 1D), it is proposed that these observations indicate spontaneous activation of αIIbβ3-L718P in resting platelets.

ADP-activated platelets from healthy volunteers, on the other hand, bound to PAC-1 with a very high affinity (Fig 3B, red lines and 3B, top panel), as expected. In contrast, only a small increase of affinity to PAC-1 was observed in ADP-treated platelets carrying the β3-L718P mutation, resulting in a marginal increase of binding potential (bottom panel). These findings suggest that αIIbβ3-L718P is partially activated in the absence of inside-out signals such as ADP, but nevertheless cannot be fully activated in the presence of such signals.

To confirm the contribution of the integrin β3-L718P mutation to spontaneous activation of αIIbβ3, CHO cells were transiently transfected with expression vectors encoding integrin β3-WT, -L718P, -D723H or -T562N together with a vector encoding αIIb-WT. Flow cytometric analysis (Fig 3C) revealed that αIIbβ3-L718P expressed in CHO cells bound to PAC-1 to the same degree as αIIbβ3-D723H, a mutant previously reported to partially activate αIIbβ3, and to a lesser extent than a fully active αIIbβ3-T562N mutant (Kashiwagi *et al*, 1999). We calculated the activation indices (see *Materials and methods*) (Hughes *et al*, 1996; Schaffner-Reckinger *et al*, 2009) of αIIbβ3-L718P and -D723H as 0·23 ± 0·07 and 0·16 ± 0·02, respectively, taking αIIbβ3-T562N as fully active (=1·0) and αIIbβ3-WT as inactive (=0) (Fig 3D). Because CHO cells were not stimulated by ADP in this experiment, each index represents αIIbβ3 activation status at rest.

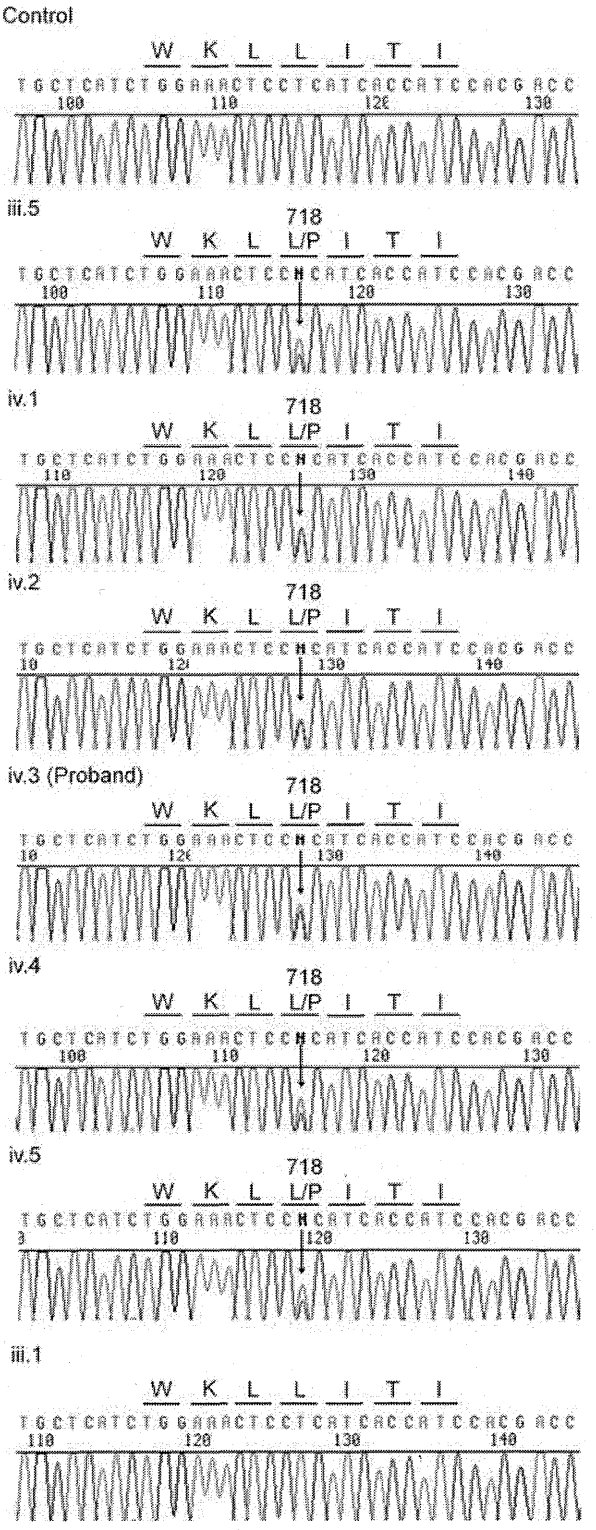

Fig 2. Direct sequencing analysis around T2231 in exon 14 of the *ITGB3* gene. Genomic DNA extracted from the affected and unaffected individuals of the pedigree were amplified by polymerase chain reaction and sequenced. Arrows indicate the position of the T2231 mutation in the *ITGB3* gene.